

## The VMC survey

### I. Strategy and first data

M.-R. L. Cioni<sup>1,2,\*</sup>, G. Clementini<sup>3</sup>, L. Girardi<sup>4</sup>, R. Guandalini<sup>1</sup>, M. Gullieuszik<sup>5</sup>, B. Miszalski<sup>1</sup>, M.-I. Moretti<sup>6</sup>, V. Ripepi<sup>7</sup>, S. Rubele<sup>4</sup>, G. Bagheri<sup>1</sup>, K. Bekki<sup>8</sup>, N. Cross<sup>9</sup>, W. J. G. de Blok<sup>10</sup>, R. de Grijs<sup>11</sup>, J. P. Emerson<sup>12</sup>, C. J. Evans<sup>13</sup>, B. Gibson<sup>14</sup>, E. Gonzales-Solares<sup>15</sup>, M. A. T. Groenewegen<sup>5</sup>, M. Irwin<sup>15</sup>, V. D. Ivanov<sup>16</sup>, J. Lewis<sup>15</sup>, M. Marconi<sup>7</sup>, J.-B. Marquette<sup>17,18</sup>, C. Mastropietro<sup>19</sup>, B. Moore<sup>20</sup>, R. Napiwotzki<sup>1</sup>, T. Naylor<sup>21</sup>, J. M. Oliveira<sup>22</sup>, M. Read<sup>9</sup>, E. Sutorius<sup>9</sup>, J. Th. van Loon<sup>22</sup>, M. I. Wilkinson<sup>23</sup>, and P. R. Wood<sup>24</sup>

(Affiliations can be found after the references)

Received 12 November 2010 / Accepted 16 December 2010

#### ABSTRACT

**Context.** The new VISual and Infrared Telescope for Astronomy (VISTA) has started operations. Over its first five years it will be collecting data for six public surveys, one of which is the near-infrared  $YJK_s$  VISTA survey of the Magellanic Clouds system (VMC). This survey comprises the Large Magellanic Cloud (LMC), the Small Magellanic Cloud, the Magellanic Bridge connecting the two galaxies and two fields in the Magellanic Stream.

**Aims.** This paper provides an overview of the VMC survey strategy and presents first science results. The main goals of the VMC survey are the determination of the spatially-resolved star-formation history and the three-dimensional structure of the Magellanic system. The VMC survey is therefore designed to reach stars as faint as the oldest main sequence turn-off point and to constrain the mean magnitude of pulsating variables such as RR Lyrae stars and Cepheids. This paper focuses on observations of VMC fields in the LMC obtained between November 2009 and March 2010. These observations correspond to a completeness of 7% of the planned LMC fields.

**Methods.** The VMC data are comprised of multi-epoch observations which are executed following specific time constraints. The data were reduced using the VISTA Data Flow System pipeline with source catalogues, including astrometric and photometric corrections, produced and made available via the VISTA Science Archive. The VMC data will be released to the astronomical community following the European Southern Observatory's Public Survey policy. The analysis of the data shows that the sensitivity in each wave band agrees with expectations. Uncertainties and completeness of the data are also derived.

**Results.** The first science results, aimed at assessing the scientific quality of the VMC data, include an overview of the distribution of stars in colour-magnitude and colour-colour diagrams, the detection of planetary nebulae and stellar clusters, and the  $K_s$  band light-curves of variable stars.

**Conclusions.** The VMC survey represents a tremendous improvement, in spatial resolution and sensitivity, on previous panoramic observations of the Magellanic system in the near-infrared, providing a powerful complement to deep observations at other wavelengths.

**Key words.** magellanic clouds – infrared: stars – stars: variables: Cepheids – stars: variables: RR Lyrae – Hertzsprung-Russell and C-M diagrams – survey

### 1. Introduction

The cosmological paradigm for the formation and evolution of galaxies suggests that large structures formed as a sequence of mergers of smaller objects (White & Frenk 1991). The theoretical framework relies on cold dark matter simulations and is supported by high redshift observations (York et al. 2000) and by studies of the cosmic microwave background (Spergel et al. 2003), but the major difficulty is to reproduce the baryonic (stars, gas and dust) content of the Universe. Therefore, the study of the assembly process of nearby galaxies via resolved stars is a crucial aspect to understand how structures in the Universe form and evolve (Tolstoy et al. 2009). In particular, dwarf irregular galaxies are well suited because their low metallicity and high gas content provide information about galaxies at an early stage of evolution. The closest prototypes of interacting dwarf galaxies that offer an excellent laboratory for this near-field cosmology are the Magellanic Clouds (MCs).

The Magellanic system is located at a distance of  $\sim 57$  kpc (e.g. Cioni et al. 2000) and comprises: the Large Magellanic Cloud (LMC), the Small Magellanic Cloud (SMC), the Magellanic Bridge and the Magellanic Stream. The LMC is a dwarf irregular galaxy seen nearly face-on (e.g. van der Marel & Cioni 2001) and sometimes referred to as a late-type spiral galaxy, rich in gas and actively forming stars. The SMC is a highly inclined dwarf irregular galaxy also referred to as a dwarf spheroidal galaxy (Zaritsky et al. 2000) with less active star formation. The LMC is probably just a few kpc thick along the line-of-sight, but the SMC has a more complex structure that may extend up to 20 kpc along the line-of-sight (e.g. Westerlund 1997; Groenewegen 2000; Subramanian & Subramaniam 2009a). There is a bar embedded in each galaxy (Subramanian & Subramaniam 2009b; Gonidakis et al. 2009). The Magellanic system is metal-poor, the metallicity is about 1/2, 1/4 and 1/10 that of the Sun for the LMC, SMC and the Bridge, respectively. The MCs have experienced an extended star formation history (e.g. Hill et al. 2000; Zaritsky et al. 2002,

\* Research Fellow of the Alexander von Humboldt Foundation.

2004; Cole et al. 2005; Pompéia et al. 2008; Gallart et al. 2008; Carrera et al. 2008).

The dynamical interaction between the MCs may be responsible for the various episodes of star formation (Zaritsky & Harris 2004) and for the creation of the Bridge (Irwin et al. 1985; Gordon et al. 2009) which connects the two galaxies and clearly has young stars associated with it (Irwin 1991; Battinelli & Demers 1998). The Stream appears (to date) as a purely gaseous feature spanning more than 100 deg in the Southern sky (Guhathakurta & Reitzel 1998). A tidal origin of the Stream from the interaction between the LMC and the Milky Way (MW) has been ruled out by new proper motion measurements (Kallivayalil et al. 2006a,b). Alternative explanations are: ram pressure (Mastropietro et al. 2005) and tidal origin from the interaction between the LMC and the SMC (Besla et al. 2010).

The interaction between the MCs and the MW is representative of the environmental effects that large galaxies with satellites (low-mass dwarf galaxies) experience elsewhere in the Universe. This suggests that the MCs may have entered the Local Group as part of an association (cf. Tully et al. 2006; Moss 2006; Knebe et al. 2006) and that, in the future, a minor merger between the LMC and the MW may occur (cf. Ibata et al. 1994, 2003). An alternative is that the MCs may be tidal dwarfs expelled during a previous merger event involving M 31 (Yang & Hammer 2010), although this would imply they have retained little dark matter from their parent halos (Barnes & Hernquist 1992). At present, basic assumptions are being challenged: What is the origin of the MCs? Do the MCs constitute a binary system and, if so, for how long? Have the MCs interacted with the MW or are they on their first approach (Besla et al. 2007; D’Onghia & Lake 2008)? How have the star-formation histories of the LMC and the SMC been influenced by interaction? Does the geometry of the system depend on age and metallicity? How do star clusters form and evolve in the MCs? What is the fate of the MCs and will they merge with the MW? Will the Bridge evolve into a dwarf galaxy (Nishiyama et al. 2007)? Does the LMC have an ordinary bar and how does it influence the LMC evolution? Or, is the offset bar a separate galaxy being merged into the LMC disc? Does the LMC have a metal poor old halo? Why is there a significant difference in structure between the gas and stars in the SMC? Does the SMC have a bulge?

To answer all these questions we must resolve the stellar populations and study them in detail. A fundamental step in this direction has been the many panoramic imaging surveys that have provided multi-wavelength observations of the Magellanic system. Except for the dedicated optical MCPS survey (Zaritsky et al. 2002, 2004) information about the overall population of the MCs has been obtained from surveys with different original goals, including microlensing optical surveys (e.g. MACHO – Alcock et al. 2000, EROS – Tisserand et al. 2007, and OGLE – Udalski et al. 1992), and infrared sky surveys (e.g. IRAS – Schwering 1989, 2MASS – Skrutskie et al. 2006, and DENIS – Cioni et al. 2000). A continuation of OGLE is still in progress while other large-scale, near-infrared (near-IR) surveys (IRSF – Kato et al. 2007) offer somewhat more sensitive data than 2MASS. The surveys in the mid-infrared with the *Spitzer Space Telescope* (SAGE – Meixner et al. 2006; Bolatto et al. 2007; Gordon et al. 2009; Bonanos et al. 2010) of the central part of the galaxies and an optical survey of the outermost regions (Saha et al. 2010) have recently been completed. These surveys have provided data covering most of the electromagnetic spectrum, but their common depth is limited to moderately bright giant stars. The development of the VISual and Infrared Survey Telescope for Astronomy (VISTA –

Emerson & Sutherland 2010) offers a unique opportunity to acquire near-IR data of unprecedented sensitivity in the Magellanic system. This is the underlying objective of the near-IR *YJK<sub>s</sub>* VISTA survey of the Magellanic Clouds system (VMC).

This paper is organised as follows. Section 2 introduces the VMC survey and then describes the observing strategy and first observations. Section 3 describes the data reduction steps for producing images and catalogues for individual observations, while Sect. 4 describes the subsequent stages of reduction for deep and linked observations and presents the archival procedures. Section 5 shows results from the first data. Section 6 concludes this study and the Appendix gives the coordinates of the VMC fields.

## 2. VMC survey

The VMC<sup>1</sup> is a uniform and homogeneous survey of the Magellanic system in the near-IR with VISTA. The main parameters of the survey are summarised in Table 1. It is the result of a letter of intent submitted in 2006 and a science and management plan approved early in 2008. The main science goals of the survey are the determination of the spatially-resolved star-formation history (SFH) and the three-dimensional (3D) structure of the Magellanic system. VMC observations will detect stars encompassing most phases of evolution: main-sequence stars, subgiants, upper and lower red giant branch (RGB) stars, red clump stars, RR Lyrae and Cepheid variables, asymptotic giant branch (AGB) stars, post-AGB stars, planetary nebulae (PNe), supernova remnants (SNRs), etc. These different populations will help assess the evolution of age and metallicity within the system.

The SFH will be recovered from the analysis of colour-magnitude diagrams (CMDs) and simulations of the observed stellar populations, accounting for foreground stars and extinction. Kerber et al. (2009) show a preliminary assessment of the SFH accuracy that can be expected from VMC data. Modelling near-IR colours bears no greater uncertainty than optical colours and the near-IR is particularly sensitive to the colour of the oldest turn-off stars. The 3D geometry will be derived using different density and distance indicators like the luminosity of red clump stars and the Cepheid and RR Lyrae period-luminosity relation, and period-luminosity-colour and Wesenheit relations. These results will complement those based on 2MASS data for the AGB and upper RGB populations of the LMC (van der Marel 2001) and those from optical data of the central regions of the galaxies that are affected by a higher reddening (e.g. Subramanian & Subramanian 2010) and crowding. We will constrain the epoch of formation of each galactic component by mapping the extent of different kinds of stars and deriving, using up-to-date stellar evolutionary models, ages and metallicities. The VMC survey science addresses many other issues in the field of star and galaxy formation and evolution, such as: stellar clusters and streams; extended sources; proper motions; star formation; distance scale; models of Magellanic system evolution; extinction mapping.

### 2.1. The VISTA telescope and camera

VISTA is a new 4 m class telescope developed in the United Kingdom (UK). It formed part of the in-kind contribution of the UK to joining the European Southern Observatory (ESO). The telescope has an alt-azimuth mounting and is located just 1.5 km

<sup>1</sup> <http://star.herts.ac.uk/~mcioni/vmc>

**Table 1.** VMC survey parameters.

Filter	<i>Y</i>	<i>J</i>	<i>K<sub>s</sub></i>	Filter	<i>Y</i>	<i>J</i>	<i>K<sub>s</sub></i>
Central wavelength ( $\mu\text{m}$ )	1.02	1.25	2.15	Exposure time per epoch (s)	800	800	750
Bandwidth ( $\mu\text{m}$ )	0.10	0.18	0.30	Number of epochs	3	3	12
Detector Integration Time – DIT (s)	20	10	5	Total exposure time (s)	2400	2400	9000
Number of DITs	4	8	15	Predicted sensitivity per epoch (Vega mag)	21.3	20.8	18.9
Number of exposures	1	1	1	Signal-to-noise per epoch at depth required	5.7	5.9	2.9
Micro-stepping	1	1	1	Total predicted sensitivity (Vega mag)	21.9	21.4	20.3
Number of Jitters	5	5	5	Total signal-to-noise at depth required	10	10	10
Paw-prints in tile	6	6	6	Saturation limit (Vega mag)	12.9	12.7	11.4
Pixel size (arcsec)	0.339	0.339	0.339	Area ( $\text{deg}^2$ )	184	184	184
System <i>FWHM</i>	0.51	0.51	0.51	Number of tiles	110	110	110

**Notes.** Jitter pattern = *Jitter5n*. Tile pattern = *Tile6zz*.

from the Very Large Telescope (VLT) site. The VISTA infrared camera (VIRCAM) is equipped with an array of 16 Raytheon detectors with a mean pixel size of  $0.339''$  and a field of view of  $1.65 \text{ deg}^2$ . The VIRCAM has a set of broad-band filters: *Z*, *Y*, *J*, *H* and *K<sub>s</sub>* and a narrow-band filter at  $1.18 \mu\text{m}$ . The point spread function of the system is specified to have 50% of the light from a point source contained within a circle of diameter  $0.51''$ . The telescope and its camera are described by Emerson et al. (2006) and Dalton et al. (2006), while the performance during commissioning is presented by Emerson et al. (2010). The science verification programmes are summarised by Arnaboldi et al. (2010).

VISTA is the largest wide-field near-IR imaging telescope in the world and it is designed to perform survey observations; at present there are six Public Surveys underway<sup>2</sup>. VISTA observes a continuous area of sky by filling in the gaps between the detectors using a sequence of six offsets, each by a significant fraction of a detector. The combined image corresponds to a VISTA *tile* that covers  $\sim 1.5 \text{ deg}^2$ , while individual offset positions are named *paw-prints* and cover an area of  $0.59 \text{ deg}^2$ . The resulting VISTA tile observes each part of sky within it at least twice, except for two edge strips in the extreme “Y” directions of the array. The tiling process for the VMC survey ensures that adjacent tiles overlap sufficiently to provide two observations of these areas as well. The combination of offsets generates small overlapping areas with exposures as large as six times a single paw-print. These steps are described in the VISTA user manual<sup>3</sup>.

The VMC survey is a near-IR *YJK<sub>s</sub>* survey of the Magellanic system. Compared to previous surveys using the 2MASS and DENIS telescopes, the choice of VISTA filters for the VMC survey was driven by the following considerations. A total of three filters were chosen to be able to analyse colour–colour diagrams. The availability of a large colour spacing to allow for a good characterisation of the subgiant branch population to derive the SFH. The relation between *J* – *H* and *J* – *K<sub>s</sub>* is quite linear for MC giants, so observations in the *H* band would have provided very little information and priority was given to a bluer filter. The *J* band was preferred over *H* as it also suffers less from atmospheric effects, and provides comparative observations with respect to previous surveys. The choice of *Y* over *Z* was motivated by a reduced confusion limit. The *K<sub>s</sub>* filter was required to determine the average magnitude of variable stars that, at this wavelength, obey a clear period-magnitude relation that is

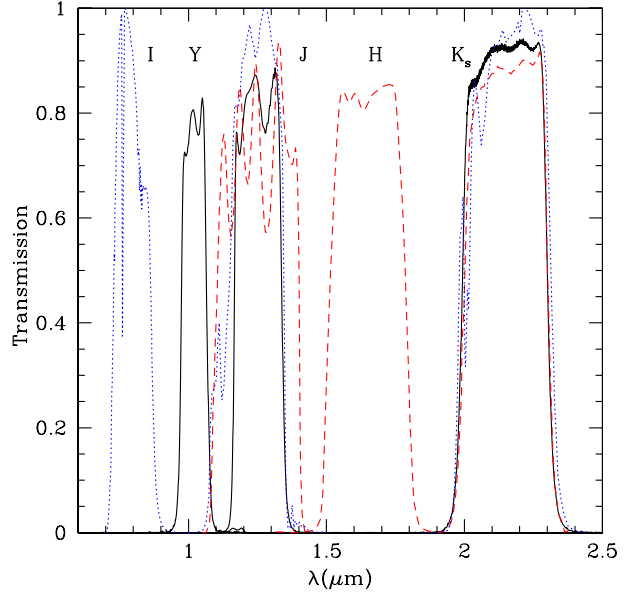


**Fig. 1.** Filter transmission curves for the VMC survey (*YJK<sub>s</sub>* – black continuous lines) compared with the transmission of the 2MASS (*JHK* – red dashed lines) and DENIS (*IJK<sub>s</sub>* – blue dotted lines) surveys.

unaffected by other stellar parameters that degrade the relation at bluer wavelengths (Sect. 5.2). A comparison among the filter transmission curves for the VMC, 2MASS and DENIS observations is shown in Fig. 1. The exposure time for the VMC survey (Table 1) is designed to meet the two key scientific objectives: the SFH and the 3D geometry. An accurate determination of the SFH requires CMDs reaching the oldest main sequence turn-off, to allow for sampling of different stellar populations. The investigation of RR Lyrae stars and Cepheids requires monitoring observations across specific time intervals. The stacking of the observations that are needed for deriving the mean magnitude of variable stars in the *K<sub>s</sub>* band meets also the depth requirement for the SFH. The split of epochs in the *Y* and *J* filters is instead purely driven by scheduling requirements.

## 2.2. VMC area coverage

Observing the entire Magellanic system extending over hundreds of kpc (the Stream covers half the sky) is a daunting task. The VMC survey concentrates, therefore, on a moderately extended area ( $\sim 180 \text{ deg}^2$ ) that includes the classical diameter limit

<sup>2</sup> <http://www.eso.org/sci/observing/policies/PublicSurveys/discretionary-sciencePublicSurveys.html>

<sup>3</sup> <http://www.eso.org/sci/facilities/paranal/instruments/vista/doc/>

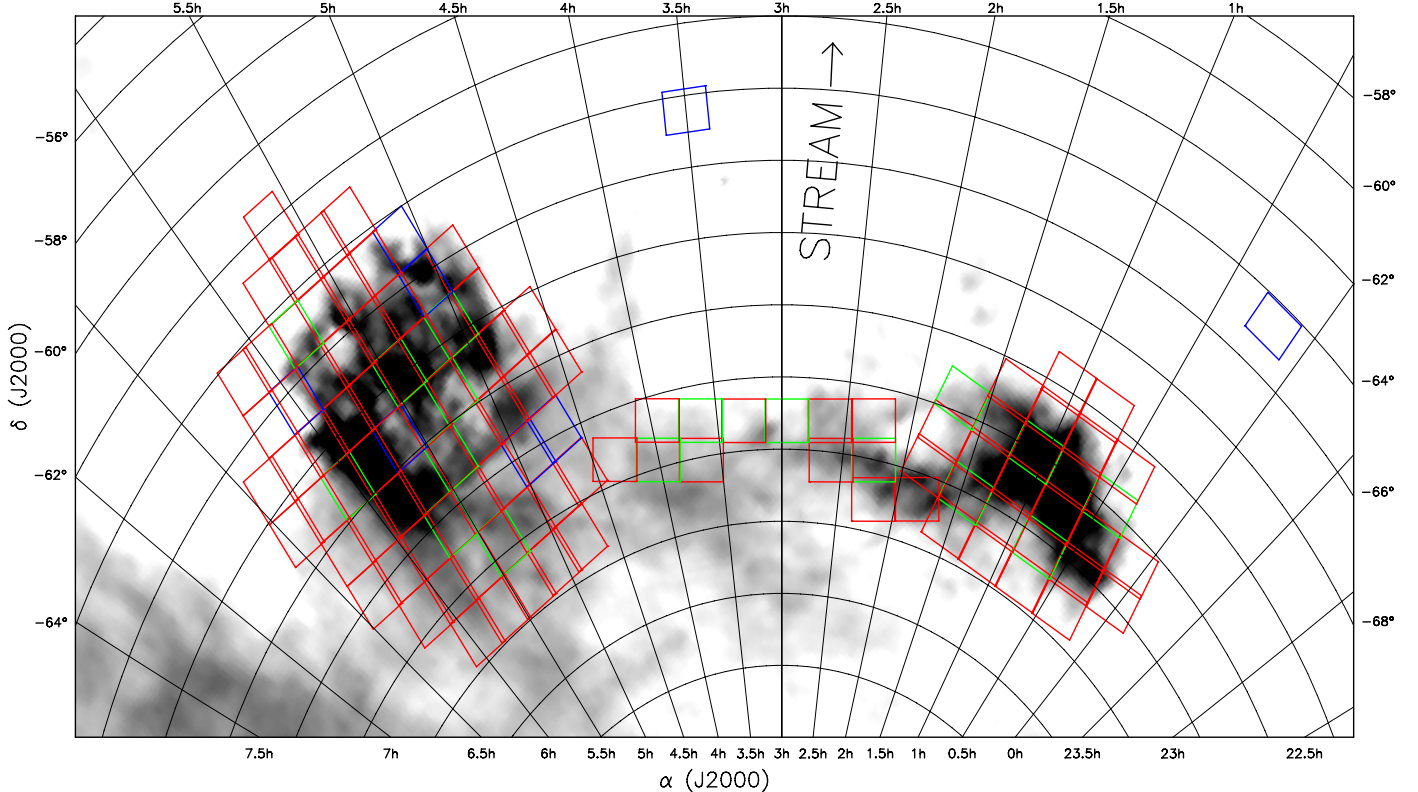


**Fig. 2.** Magellanic system area tiled for VMC observations. The underlying image shows the HI distribution (McClure-Griffiths et al. 2009). VISTA tiles are colour coded as follows. Blue rectangles represent tiles for which observations have started during the dry-runs and P85, green rectangles are for tiles with observations in P86, and red tiles are observations that will not be before P87.

at  $B \approx 25$  mag arcsec $^{-2}$  for both galaxies (Bothun & Thompson 1988) as well as major features traced by the distribution of stars (e.g. Irwin 1991; Bica et al. 2008) and HI gas (e.g. Staveley-Smith et al. 2003; Hatzidimitriou et al. 2005; Muller et al. 2003), the Bridge and two fields at specific locations in the Stream.

The LMC area ( $116$  deg $^2$ ) is covered by 68 tiles, while 27 tiles cover the SMC ( $45$  deg $^2$ ) and 13 cover the Bridge ( $20$  deg $^2$ ), see Fig. 2. Additionally, 2 tiles ( $3$  deg $^2$ ) are positioned in the Stream, one approximately to the North of the centre of the Bridge (corresponding to a dense area of gas) and the other, at similar right ascension, to the North of the SMC, corresponding to a dense area of stars following the simulations by Mastropietro (2009). VMC tile centre coordinates are given in the Appendix. Each tile is identified by two numbers: the first number indicates the row and the second the column of the position of the tile in the mosaic that covers the system. Note that a separate tiling pattern has been defined for each region (Figs. A.1, A.2, A.3). Row numbers increase from South to North and column numbers increase from West to East.

Tiles covering the LMC were oriented at a position angle of +90 deg. The default orientation (position angle = 0 deg) points the “Y” axis to the North and the “X” axis to the West. The position angle is defined to increase from North to East. This represents the best compromise between minimum number of tiles and maximum area, increasing the efficiency of the survey. The overlap between the doubly-covered sky areas in adjacent tiles corresponds to 60” in both “X” and “Y” directions. The LMC mosaic was created using the Survey Area Definition Tool (SADT – Arnaboldi et al. 2008). A geodesic rectangle centred at  $\alpha = 05:35:50$ ,  $\delta = -69:27:12$  (J2000), with width = 11.8 deg and height = 15.9 deg, was created as the basis of the tiling process.

Outer tiles were removed leading to the pattern shown in Fig. 2 (see also Fig. A.1). The area covered by the tiles was checked against the distribution of stellar associations, carbon stars and other stellar objects using Aladin (Bonnarel et al. 2000). The centre of the rectangle was adjusted to include the 30 Doradus nebulosity within a single tile and, similarly, the field that the future space mission Gaia<sup>4</sup> will repeatedly observe for calibration.

In the process of creating the mosaic, SADT requires as input the observing parameters that are associated to small (i.e. jittering) and large (i.e. mosaicking) displacements in the tile position. For the VMC survey the maximum jitter was set to 15”, the *backtrackStep* to 100 and the tiling algorithm to *Tile6zz* (these parameters are described in the SADT user manual). Guide stars were assigned automatically to each tile using the GSC-2 reference catalogue (Lasker et al. 2008). This process may result in shifting the tile centre in case an insufficient number of reference stars is available, but this was not the case for LMC tiles.

Tiles covering the SMC region were placed at a position angle of 0 deg. Keeping the wide tile-edge approximately along the right ascension direction produces maximum coverage for a minimum number of tiles. This also implies centring the geodesic rectangle at  $\alpha = 00:50:00$ ,  $\delta = -73:00:00$  (J2000), with width = 8.0 deg and height = 8.0 deg. This rectangle represents the basis of the tiling process and outer tiles were subsequently removed leading to the pattern shown in Fig. 2 (see also Fig. A.2). As before, the area covered by tiles was checked against the distribution of different stellar objects. The position of the centre of the rectangle was tuned to match the area that

<sup>4</sup> <http://sci.esa.int/science-e/www/area/index.cfm?fareaid=26>

will be observed in the optical domain by the VST<sup>5</sup> (VLT Survey Telescope) as part of the STEP survey (P.I. Ripepi; Capaccioli et al. 2005) and to provide sufficient overlap for a consistent calibration with the Bridge area.

Previous observations of the Magellanic Bridge by Battinelli & Demers (1992) and Harris (2007) covered fields departing from the LMC and tracing arcs at different declinations with only a few fields between the two. In order to maximise the total population of stars that the VMC survey will detect the 2MASS, DENIS and SuperCOSMOS<sup>6</sup> databases were explored for stellar densities and compared with the previous observations. VMC tiles were then positioned to overlap with the area that provides a good sampling of the stellar population while also following a continuous pattern. Following a similar procedure for the LMC and SMC areas, a geodesic rectangle was drawn with centre at  $\alpha = 03:00:00$ ,  $\delta = -74:30:00$  (J2000), with width 13.5 deg and height 3 deg. Outer tiles were subsequently removed leading to the pattern shown in Fig. 2 (see also Fig. A.3).

The two tiles positioned in the Stream region were prepared using the same parameters as for LMC tiles, except for the position angle set to 0 deg. Two geodesic rectangles centred on the two fields were defined, each with a default size equal to a single tile.

### 2.3. VMC observations

The VMC data described here were mostly obtained during Science Verification observations (15–31 October 2009) and the so-called dry-run period (1 November 2009–31 March 2010) when VISTA was tested and survey operations were still being defined. A small amount of data was also taken during ESO Period 85 (1 April 2010–30 September 2010). The bulk of the VMC observations will be carried out during the even-numbered ESO periods starting in October every year and ending in March the following year because of the seasonal observability of the Magellanic system.

Observations of the VISTA Public Survey are obtained in service mode by ESO staff. This guarantees efficiency of operations and a high level of data homogeneity. The requested observing conditions for the VMC survey are summarised in Table 2. A dozen tiles, centred on the most crowded regions i.e. 30 Dor and the central regions of both LMC and SMC, have more stringent seeing conditions. This is necessary to prevent confusion in the bluest bands, while  $K_s$  band observations will not be limited by confusion for a seeing  $\leq 0.9''$ . The best  $FWHM$ s in the VISTA images are 0.6–0.7'' and undersampling, with respect to a pixel size of 0.339'', is not a cause of concern in the data treatment.

The Magellanic system never rises above 50° from the horizon. Therefore, a compromise had to be made between observing at reasonable airmass and achieving continuous observability over about five months for the monitoring process. The maximum airmass constraints were optimised as a function of the tile declination, as shown in Table 2. A violation of any observing constraint by 10% is still considered as if observations were obtained within specifications. It is also assumed that the airmass constraint may be violated by more than 10% provided the seeing constraint is not.

Table 1 describes the main parameters of the VMC observations. The total exposure time is calculated as follows: (number of epochs)  $\times 2 \times$  (number of jitters)  $\times$  (number of DITs)  $\times$  DIT.

**Table 2.** VMC required weather conditions.

Band	Seeing (arcsec) uncrowded	Seeing (arcsec) crowded
$Y$	1.2	1.0
$J$	1.1	0.9
$K_s$	1.0	0.8
Field	Tile row	Airmass
LMC	2, 3, 4	1.7
LMC	5, 6, 7	1.6
LMC	8, 9, 10, 11	1.5
Stream	1, 2	1.5
SMC	2, 3, 4, 5	1.7
SMC	6, 7	1.6
Bridge	1, 2, 3	1.7

**Notes.** Moon distance  $>80$  deg. Sky transparency = variable, thin cirrus.

**Table 3.** VMC survey progress.

Description	VMC all	LMC all	LMC season I
Total number of tiles	110	68	6
Total number of epochs	1980	1224	108
Total number of $Y$ -band epochs	330	204	18
Total number of $J$ -band epochs	330	204	18
Total number of $K_s$ -band epochs	1320	816	72
Observed number of $Y$ -band epochs	18	18	18
Observed number of $J$ -band epochs	18	18	18
Observed number of $K_s$ -band epochs	51	51	51
Total number of observed epochs	87	87	87
Completion in the $Y$ -band	5.4%	8.8%	100%
Completion in the $J$ -band	5.4%	8.8%	100%
Completion in the $K_s$ -band	3.9%	6.2%	71%
Total completion	4.4%	7.1%	80%

The factor of two comes from the tiling pattern, during which most points of the sky are observed twice (on average). The exceptions are the tile edges, observed once, and some areas of extra overlap among the detectors that are observed four or six times. For example, for the  $K_s$  band the total exposure time is:  $12 \times 2 \times 5 \times 15 \times 5 = 9000$  s.

The observations follow the nesting sequence FPJME (see VISTA User Manual<sup>7</sup>). This sequence first sets a filter, then obtains images at all jittered positions of the first paw-print, before moving to the next paw-print and taking all the jittered images at that position, and so on, until all six paw-prints that form the tile are completed. The Jittern pattern was *jitter5n* and the tile pattern was *Tile6zz*.

The progress of the VMC survey is shown in Fig. 2 and detailed in Table 3. The reader is referred to the VMC<sup>1</sup> public web page for following up the survey progress beyond that described in this paper.

#### 2.3.1. Science verification

The observation of a single paw-print in the  $YJK_s$  filters was requested during the instrument Science Verification (SV) time.

<sup>5</sup> <http://vstportal.oacn.inaf.it/>

<sup>6</sup> <http://surveys.roe.ac.uk/ssa/index.html>

<sup>7</sup> <http://www.eso.org/sci/facilities/paranal/instruments/vista/doc/>

The main goal was to verify the observing strategy and to test the saturation limits for the adopted DITs of 6, 10 and 20 s in the  $K_s$ ,  $J$  and  $Y$  bands, respectively. The observations were carried out on the night of 17 October 2009, but the data were only available after the dry-runs had started.

The SV data indicate that the saturation limit varies from one detector to another. On average, it is 11.6 mag for the 6 s  $K_s$  band exposure, with seeing of 0.94''. The linearity is mild at 11.6 mag, but becomes severe for point sources brighter than 10.7 mag. These limiting magnitudes are somewhat fainter than predicted. Prior to the beginning of the dry-runs it was decided to reduce the  $K_s$  band DIT down to 5 s, which improves the photometry of the bright stars and maximises the range of overlapping magnitudes with 2MASS. The observing strategy was then established and no modification was needed for the observations that had already started.

Other SV observations were obtained on 28 Nov. 2009 in the SMC. These are  $K_s$  band observations of one tile, with a six paw-print mosaic and DIT = 10 s, with the purpose of checking the sky-subtraction procedures. Images were obtained to test an off-sky algorithm which is not applicable to VMC data. In addition, some 2MASS touchstone fields that are observed for photometric checks are located in the VMC survey area, providing extra, albeit shallow (DIT = 5 s), multi-epoch data in all VIRCAM filters.

### 2.3.2. Dry-runs during 1 November 2009 – 14 February 2010

One hundred hours of VMC observations were submitted for execution during the 1 November 2009–14 February 2010 dry-run period and 70% were executed. Tables 4 and 5 summarise the observations where each date corresponds to the observing date of one observing block (OB). Each VMC OB includes only one filter. These observations were prepared using a new version of the Phase II Proposal Preparation<sup>8</sup> tool especially revised for Public Surveys with the VISTA and VST telescopes. It allows the user to have more control over the survey execution with new high-level tools called *scheduling containers* (Arnaboldi et al. 2008). Three types of containers were available: *concatenations* (grouping together OBs for back-to-back execution), *time-links* (imposing time constraints for the execution of OBs, including execution of OBs in a user-defined sequence), and *groups* (that improve the prioritisation of OBs to ensure the completion of one set of OBs before another set is started).

Six VMC fields were observed in the LMC (Fig. 2). One field covers the famous 30 Dor region (6\_6), one field corresponds to the South Ecliptic Pole (SEP) region that Gaia will observe repeatedly for calibration (8\_8), a pair of fields are located in the Northern outer part of the LMC disc (8\_3 and 9\_3, overlapping in declination) while the remaining two fields overlap in right ascension and are located towards the Bridge (4\_2 and 4\_3). The 30 Dor field was chosen because it is well studied and represents a crowded region of the LMC rich in stars and gas. The Gaia field was chosen for its importance to the Gaia mission; early analysis and release of these data will benefit the astronomical community in general. The two fields in the Northern disc were chosen to sample an uncrowded and external area of the galaxy. Those towards the Bridge satisfy a similar criterion but sample a different region of the LMC disc. Overall the six fields were also chosen to reflect different coordinates and observing conditions.

Table 4 shows the observations of concatenations and groups for each LMC field. Groups represent observations in the  $Y$  and  $J$  bands that are not linked by time, i.e. for a given field they can be executed on any night including on the same night. They are labelled  $Y1$ ,  $J1$ ,  $Y2$  and  $J2$ . Concatenated observations are preceded by the letter  $C$  and the integration time per filter is shorter than for a single VMC epoch at that filter (Table 1), but the different filters are observed back-to-back. The time limit for a concatenation, during this period, was 1.5 h. Two concatenations were, therefore, necessary for recovering one VMC epoch per filter. An important feature of concatenations is that the sky condition requirements are met during its entire duration. This is not always the case and then the concatenation has to be repeated. This explains why in Table 4 there are additional observations of OBs that are part of concatenations but without observations in all three filters. These additional observations will be used to investigate source variability and to produce deep stacks (Sect. 4) if the observing condition criteria (Table 2) were met.

Table 5 shows time-link sequences where 11 individual  $K_s$  band OBs are associated with each LMC field. Each sequence can start at any time, independent of the execution of observations listed in Table 4, i.e. a  $TK1$  OB can be observed on the same night as an OB in the  $Y$ ,  $J$  or  $K_s$  filter taken as part of a concatenation or group. Once started, the next observation of a  $TKn$  OB, in a time-link sequence, is obtained at intervals equal or larger than: 1, 3, 5 and 7 days for epochs 2 to 5, respectively, and thereafter at least 17 days from each previous observation (epochs 6 to 11). Some OBs in the time-link sequence were also repeated.

### 2.3.3. Dry-runs during 15 February 2010 – 31 March 2010 and ESO Period 85

The remaining dry-run period until the end of March 2010 and the subsequent ESO survey period (P85) until the end of September 2010 were not ideally suited for observations of the Magellanic system, except for short windows at the beginning and the end of the period. The VMC survey was assigned 30 h during this period. Seven hours were scheduled to progress on the  $K_s$  monitoring of four of the six LMC fields started during the first dry-run period. The remaining hours were for observations of the fields in the Stream. The overall observation of the LMC fields during the dry-runs and P85 bring the completion rate of the six fields to 80%.

The strategy for the fields in the Stream was changed because concatenations were limited to a total execution of time of 1 h. This limit imposes a further subdivision of the VMC epochs that may increase the observing overheads. We have decided to adopt a different procedure that keeps the overheads more or less constant and does not interfere with the requirement of observing different filters as close in time as possible. In the new approach there are 3 concatenations per field and each one contains only two filters:  $YJ$ ,  $YK_s$  and  $JK_s$ . The sum of the integration times per filter is the same as that from the two previous concatenations and it is also the same as a VMC epoch. The first observations of the Stream will be described in a subsequent paper of this series.

## 3. Data reduction

The raw VISTA images acquired for the VMC survey were reduced by the VISTA Data Flow System (VDFS) pipeline at the Cambridge Astronomical Survey Unit (CASU)<sup>9</sup>. The VDFS

<sup>8</sup> <http://www.eso.org/sci/observing/phase2/P2PP/P2PPSurveys.html>

<sup>9</sup> <http://casu.ast.cam.ac.uk/surveys-projects/vista>

**Table 4.** LMC epochs: concatenations ( $C$ ) and  $YJ$  bands.

Tile	$CK1$	$CJ1$	$CY1$	$CK2$	$CJ2$	$CY2$	$Y1$	$J1$	$Y2$	$J2$
4_2	20.12.09	20.12.09 <sup>b</sup>	20.12.09 <sup>b</sup>	15.01.10 4.01.10	15.01.10 4.01.10	15.01.10 4.01.10	15.12.09	14.11.09	16.12.09	28.11.09 15.12.09
4_3	23.12.09 22.12.09	23.12.09 <sup>a</sup> 22.12.09	23.12.09 22.12.09	16.01.10 <sup>b</sup> 16.01.10	16.01.10 16.01.10	16.01.10 16.01.10	9.12.09	18.11.09	10.12.09	28.11.09
6_6	5.11.09	5.11.09	5.11.09	20.11.09 26.11.09	20.11.09 9.11.09	20.11.09 9.11.09	4.11.09	4.11.09	8.11.09	8.11.09
8_3	26.11.09	26.11.09	26.11.09	22.11.09 26.11.09	22.11.09 26.11.09	22.11.09 26.11.09	19.11.09	15.11.09	21.11.09	26.11.09
8_8	21.11.09 26.11.09	21.11.09	21.11.09	20.11.09 26.11.09	20.11.09 26.11.09	20.11.09 26.11.09	5.11.09 6.11.09 <sup>b</sup>	9.11.09 7.11.09 <sup>b</sup>	9.11.09 11.11.09	11.11.09
9_3	21.11.09	21.11.09	21.11.09	22.11.09	22.11.09	22.11.09 <sup>b</sup>	30.11.09	1.12.09	1.12.09	2.12.09

**Notes.** <sup>(a)</sup> Reduced number of jitters and/or paw-prints. <sup>(b)</sup> Seeing and/or ellipticity too high.

**Table 5.** LMC epochs: time linked ( $T$ )  $K_s$ -band monitoring.

Tile	$TK1$	$TK2$	$TK3$	$TK4$	$TK5$	$TK6$	$TK7$	$TK8$	$TK9$	$TK10$	$TK11$
4_2	14.12.09	17.12.09	5.01.10	14.01.10	22.01.10						
4_3	10.12.09	17.12.09	21.12.09	27.12.09	18.01.10						
6_6	8.11.09 6.11.09 <sup>a</sup>	12.11.09	17.11.09	29.11.09	7.12.09	26.12.09	13.01.10 <sup>a</sup>	31.01.10	19.02.10	11.03.10	10.11.10
8_3	3.12.09	6.12.09	22.12.09	28.12.09	14.01.10	31.01.10	22.02.10	25.10.10	14.11.10 <sup>b</sup>		
8_8	14.11.09	19.11.09	25.11.09	30.11.09	7.12.09 <sup>b</sup>	25.12.09	14.01.10	31.01.10	19.02.10	08.03.10	26.11.10 16.11.10 <sup>b</sup>
9_3	4.12.09	9.12.09	19.12.09	23.01.10	31.01.10	24.02.10	15.09.10				
				16.01.10 <sup>b</sup>		20.02.10 <sup>b</sup>					

**Notes.** <sup>(a)</sup> Reduced number of jitters and/or paw-prints. <sup>(b)</sup> Seeing and/or ellipticity too high.

pipeline is specifically designed for reducing VISTA data (Irwin et al. 2004) and is used to process up to 250 GB/night of data. The pipeline is a modular design allowing straightforward addition or removal of processing stages. The VMC data are reduced together with other VISTA data on a weekly basis. Prior to this science reduction the data are checked at the observatory site (ESO Chile) using a simplified version of the VDFS pipeline and library calibrations. The data are subsequently checked at ESO in Garching for monitoring the instrument performance and to feed updated information back to the observatory.

The most relevant VDFS steps for the reduction of VMC survey data are as follows:

- reset, dark, linearity, flat and de-striping (removing horizontal stripes in the background) correction;
- sky background correction (tracking and homogenisation during image stacking and mosaicking);
- jittered and paw-print stacking;
- point source extraction;
- astrometric and photometric calibration (the latter put in an internally uniform system);
- bad pixel handling, propagation of uncertainties and effective exposure times by use of confidence maps;
- nightly extinction measurements.

The different observational uncertainties are propagated during the data processing, to give the users a clear picture of the final data quality. Various quality control parameters are calculated during the data reduction to monitor the data, and to evaluate both the observing conditions (in retrospect) during the observation, and the individual data reduction steps. Among them are: the zero-point to measure the atmospheric extinction, the  $FWHM$

to measure the seeing, the ellipticity to evaluate the quality of the guiding and active optics correction, the sky level to estimate the background level and its variations, etc. The processing history is recorded directly in FITS headers.

A tile image is produced by combining 96 different images (16 detector images per each of 6 paw-prints). Their sky level and individual paw-print astrometric and photometric distortion are adjusted in the drizzling (combination) process. Tile catalogues are produced following the application of a nebulosity filter to the paw-prints in order to remove diffuse varying background on scales of 30'' or larger (Irwin 2010). This method has shown that the detection of objects and their characterisation (astrometry, photometry and morphological classification) are considerably improved.

The first VMC reduced images and catalogues, corresponding to observations obtained during November 2009, were received in January 2010. These data were reduced with version 0.6 (v0.6) of the VDFS pipeline and refer to individual paw-prints, not yet combined into tiles. This means that in practise, for example, the observation of a  $Y$ -band OB of a given field has 6 associated images, 6 catalogues and 6 confidence maps. Each image and catalogue are delivered in Rice compressed format and are multi-extension FITS files containing each the information for all of the 16 detectors covering the VIRCAM field-of-view. In March 2010 we received more data processed with an upgraded version of the pipeline (v0.8). These data include all observations obtained until the end of January 2010. The processed observations obtained after this date and until the end of the Magellanic season (March 2010) were received in April 2010. Following quality inspection a few images were re-reduced (v0.9) to fix some specific problems with a small subset

of the data. The v0.8 data were ingested into the VISTA Science Archive (VSA) by June 2010 (Sect. 4). They include astrometry and photometry in single-band, band-merged and epoch-merged tables as well as deep stacks. In October 2010 v1.0 data have become available and the main difference from previous releases is that they include tile images and catalogues.

Figure 3 shows most of a tile of the 6\_6 LMC field including the star forming region 30 Dor. This image was produced for an ESO press release<sup>10</sup> where other zoomed-in images are also available. The exposure time in the three wave bands was 2400 s in  $Y$ , 2800 s in  $J$  and 4850 s in  $K_s$ .

### 3.1. Linearity and background

The individual VISTA detectors have different non-linearity and saturation properties and these properties may also vary across a given detector. The detector system is non-linear and linearity corrections are applied at the pixel level during the initial image processing stages. The saturation levels are stored in the image header keywords and, together with the peak flux derived from the photometry of the observed sources, it is possible to establish a correction that enables recovery of stars up to a few magnitudes brighter than the saturation limit (Irwin 2009). This correction is not implemented by VDFS prior to the production of VMC catalogues but it is applied at a further stage of the data processing (Sect. 4). The expected saturation values listed in Table 1 are sensitive to seeing variations. In fact, the 30 Dor region was observed under very good conditions, and saturation appears at fainter magnitudes.

The application of a nebulosity filter to the paw-print images prior to the construction of a tile image (Irwin 2010), may influence the recovery of the magnitude of stars close to the saturation limit. This would, however, only affect heavily saturated stars, i.e. those where a significant halo with a diameter comparable to that of the filter size ( $\sim 30''$ ) is visible.

The sky background for VMC observations is estimated, for each paw-print, from all paw-prints observed for one tile in a given band and at a given time. This method, referred to as “tilesky”, has shown very good results even for the 30 Dor tile where there is a substantial emission from the nebula.

Persistence effects due to bright stars are usually automatically removed by the VDFS pipeline when the observations, like for VMC, follow the FPJME sequence (see VISTA User Manual<sup>6</sup>). Adding up all VMC images for a given field and filter does not produce any noticeable effect due to persistence.

The moon has a negligible effect on the VMC background because it is always  $>80$  deg away from any of the fields. This results in low contamination, even in the  $Y$  band which is most susceptible to the lunar effect. The major absorption is caused by water vapour and carbon dioxide in the atmosphere. At the VMC filters the background will also be dominated by non-thermal aurora emission, OH and  $O_2$  lines especially in observations obtained 1.5–2 h after twilight.

### 3.2. Astrometry

Astrometry is based on positions of the many 2MASS sources within each detector. The astrometric calibration of a paw-print is encoded in the FITS image headers using the Zenithal Polynomial projection (ZPN) while a tile refers to a single tangent plane World Coordinate System (WCS) image (Calabretta & Greisen 2002). The median astrometric root-mean-square is

80 mas and is dominated by 2MASS uncertainties. Residual systematic distortions across the VISTA field-of-view are at the  $\sim 25$  mas level and can be further improved, if required, by directly characterising the distortion pattern. In a dithered sequence the detectors are rotated slightly to maintain the position angle on the sky; a comparison between identical VISTA observations shows a residual rotation of  $\sim 0.5$  pix.

Figure 4 shows a comparison between the right ascension ( $\alpha$ ) and declination ( $\delta$ ) coordinates of stars that are in common between VISTA and 2MASS in the VMC field 8\_8. The excellent match shows the quality of the astrometry. A systematic shift is perhaps present at the level of  $\sim 0.01''$  in both axes. This accuracy is perfectly adequate for cross-correlation studies between external catalogues and VMC. The relative accuracy within VMC data is higher and a more detailed investigation of the suitability of VMC data for studies of, for example, proper motions will be addressed elsewhere.

### 3.3. Photometry

The photometric calibration relies on the observation of stars from the 2MASS catalogue with magnitudes in the range 12–14 mag in all bands. The procedure is similar to that adopted to calibrate data from the Wide-Field Camera (WFCAM) mounted at the United Kingdom Infrared Telescope (UKIRT). For the WFCAM filters, which are very similar to VISTA’s (except that WFCAM has  $K$  and VISTA has  $K_s$ ), Hodgkin et al. (2009) have shown that the calibration of the  $Y$  band, not included in 2MASS, is possible where the extinction is not too high, i.e.  $E(B-V) < 1.5$ . This is well within the average extinction values towards the Magellanic system (Westerlund et al. 1997). However, in star-forming regions the extinction can reach larger values and the calibration may not be reliable. To remedy this situation a calibration based on the observations of standard stars will be produced together with a thorough investigation of star-forming regions from previous data.

A high quality global photometric calibration of the VMC survey will be supported by the homogeneity and accuracy of the 2MASS catalogue. The best absolute photometry is expected to be accurate to about 1% and, on average, 2%, but relative photometry will reach a much greater accuracy ( $\sim$ milli-magnitudes for brighter sources). At periodic intervals and at the end of the survey the global photometric calibration will be assessed.

Figure 5 shows the behaviour of VISTA photometric uncertainties in the VMC 8\_8 field where data represent stacked paw-prints and tiles. Note that the uncertainties reduce by about  $\sim 50\%$  compared to the individual tiles, and will reduce further for deep tiles. In the VMC catalogues several aperture flux magnitudes are given that sample the curve of growth of all images. The recommended aperture “aper3”, used in this work, corresponds to a core radius of  $1''$  (3 pixels) that contains 75% of the total stellar flux in a  $0.8''$  seeing observation.

Figure 6 shows a comparison between VMC and 2MASS\* magnitudes. By selecting a suitable range of magnitudes the parameters of the comparison (mean, median and sigma) are indicated in Table 6. Note that by 2MASS\* we do not refer to 2MASS magnitudes, but to the magnitudes obtained using the following colour equations:

$$Y_{\text{2MASS}^*} = J_{2m} + 0.550 \times (J_{2m} - H_{2m}) \quad (1)$$

$$J_{\text{2MASS}^*} = J_{2m} - 0.070 \times (J_{2m} - H_{2m}) \quad (2)$$

$$K_{\text{2MASS}^*} = K_{2m} + 0.020 \times (J_{2m} - K_{2m}) \quad (3)$$

<sup>10</sup> <http://www.eso.org/public/news/eso1033/>



**Fig. 3.** Most of VMC tile of LMC field 6\_6. This is a colour composite image where  $Y$  is shown in blue,  $J$  in green and  $K_s$  in red. East is to the left and North at the top. The 30 Doradus star forming region is visible together with other smaller regions towards the South as well as stellar clusters and the field population. For more details and a high resolution image refer to <http://www.eso.org/public/news/eso1033/>

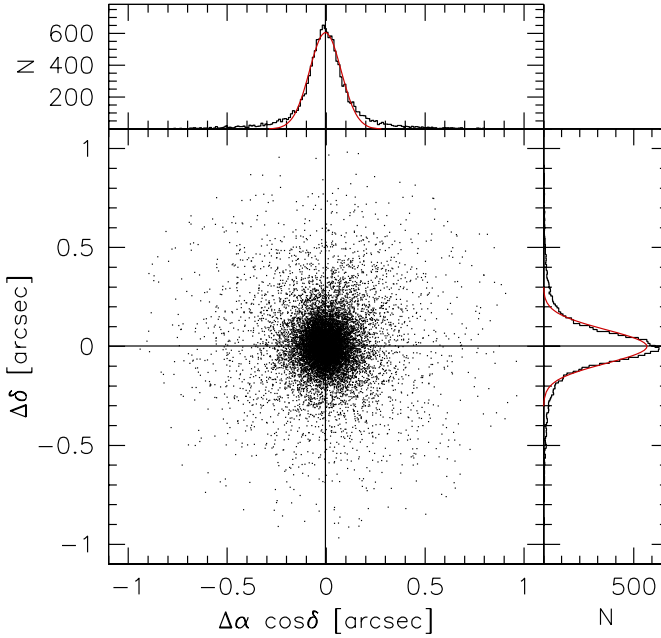


**Fig. 4.** Comparison between VISTA and 2MASS astrometry in the 8\_8 field. Histograms have bins of  $0.01''$  in size. The best fitting gaussians are indicated and correspond to  $\sigma$  of  $0.080''$  and  $0.085''$  for  $\Delta\alpha$  and  $\Delta\delta$ , respectively.

**Table 6.** VMC-2MASS\* comparison.

Band	Range (mag)	Mean (mag)	Median (mag)	Sigma (mag)
$Y$	10.5–15.0	+0.018	+0.012	0.110
$J$	10.5–14.5	-0.005	-0.003	0.092
$K_s$	10.0–14.0	-0.003	-0.003	0.069

where  $J_{2m}$ ,  $H_{2m}$   $K_{2m}$  are 2MASS magnitudes. These are the formulas used to calibrate the VISTA photometry<sup>11</sup>. They include the correct colour term but do not include the small zero-point shifts that are necessary to bring the observations into a Vega magnitude system.

The morphological classification is encoded in a flag with values: -1 for stellar, +1 for non-stellar, 0 for noise and -2 for borderline stellar sources. This classification indicates the most probable source morphology and is affected by crowding and sensitivity. For details about the photometric apertures, the source classification and other catalogue parameters the reader is referred to the CASU web pages.

### 3.4. Image quality

The quality of the VMC images is evaluated at three different steps – during the observations, the data reduction, and the archiving process. The VMC team performs additional quality control checks that interleave with each of these three steps. The first identifies obvious causes for re-observation, such as observations that exceeded the required constraints or that failed to be completed because of technical reasons. These observations are

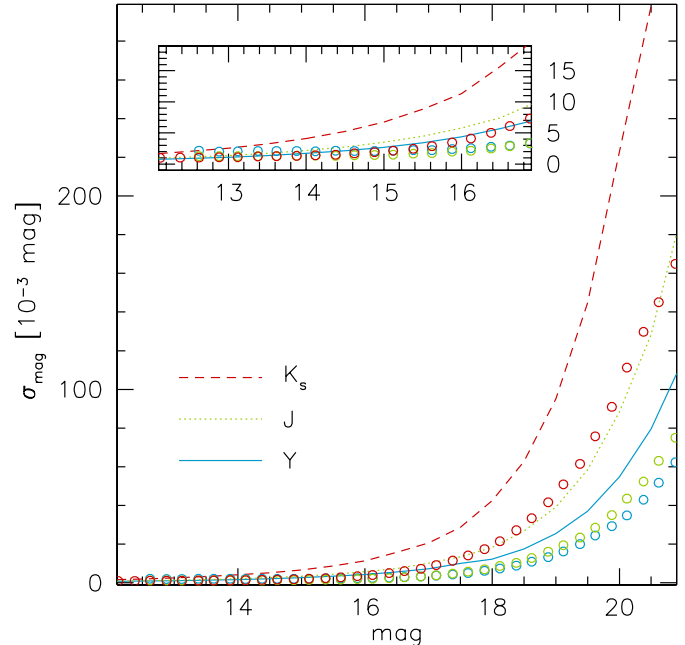


**Fig. 5.** Photometric uncertainties in the VMC data for stacked paw-prints (dashed, dotted and continuous lines in the  $K_s$ ,  $J$  and  $Y$  bands respectively) and tiles (red, green and blue circles in the  $K_s$ ,  $J$  and  $Y$  bands respectively) in the 8\_8 field. Uncertainties are progressively smaller from  $K_s$  to  $Y$  and are systematically smaller in tiles than in stacked paw-prints.

usually repeated almost immediately (Tables 4, 5). All images are processed by CASU and archived at the VSA, regardless of whether their observing constraints are met.

All CASU-reduced VMC survey images for individual detectors have been inspected visually for quality control. The purpose of this inspection is to recognise artefacts and residuals from the reduction process but also to identify features that are intrinsic to the observations. The results of the quality inspection are as follows:

- The upper 1/3 of detector #16 is effectively noisy in the bluer bands, this also causes a calibration problem for that region: so the VMC  $Y$  band observations suffer more than the  $J$  and  $K_s$  ones. This problem causes an increasing background level and influences the detection capabilities.
- The observations obtained before 20 November 2009 suffer from intermittent problems in detector #6 channel #14 (each detector has 16 channels, processed by different analog-to-digital convertors) that required replacement of a video board in the controller. These stripes cover an area comparable to that of a bright foreground star.
- A special sky frame needs to be used for reducing images obtained during the night of 19 November 2009, due to investigations on the component responsible for the previous problem. This step is implemented in the pipeline reduction from version 0.9 onwards.
- A low quality region at the bottom (“-Y”) of detector #4 creates a horizontal pattern that does not cancel out with stacking images obtained from the exposure and jittering sequence. This problem will likely not affect subsequent reductions of the data.
- Overall the reduced images show a smooth gradient most noticeable in the  $K_s$  band (possibly caused by the baffling

<sup>11</sup> <http://casu.ast.cam.ac.uk/surveys-projects/vista/technical/vista-sensitivity>

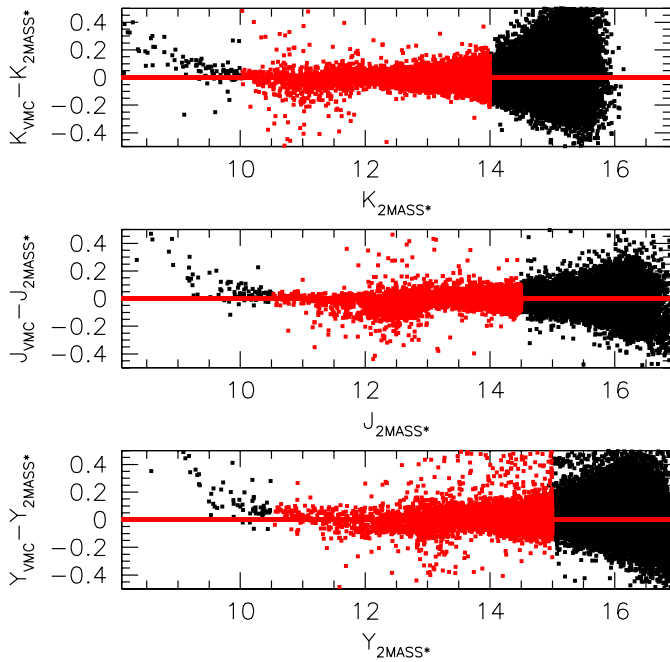


**Fig. 6.** Magnitude difference between VMC and 2MASS\* sources for stars in the 8\_8 field. Horizontal lines were defined within a specific range of magnitudes that is given in the text and is indicated in red in the colour version of the figure.

**Table 7.** Average VMC parameters from all single tile images.

Band	FWHM (arcsec)	Ellipticity	Zero – point (mag)	5 $\sigma$ Mag. Limit (mag)
<i>Y</i>	$1.03 \pm 0.13$	$0.065 \pm 0.011$	$23.520 \pm 0.070$	$21.111 \pm 0.395$
<i>J</i>	$1.00 \pm 0.10$	$0.064 \pm 0.011$	$23.702 \pm 0.206$	$20.527 \pm 0.382$
<i>K<sub>s</sub></i>	$0.93 \pm 0.08$	$0.051 \pm 0.009$	$22.978 \pm 0.245$	$19.220 \pm 0.340$

system of VIRCAM as a result of thermal radiation), but does not present a problem for the source extraction.

None of these problems require re-observation of the tiles that have been obtained for the VMC survey.

The quality of the images was further inspected by comparing the *FWHM* of the extracted sources with the expected seeing requirements. As expected the *FWHM* varies among the VIRCAM detectors. For example, the average *FWHM* in the corners of detector #1 is larger than in other detectors. This implies that some detectors will have a *FWHM* that exceeds the seeing requirement by more than 10%. The average seeing among the detectors and the average seeing among the six paw-prints of a tile is, however, always within the required limit, except in a few cases, see Tables 4 and 5.

Tables 4 and 5 also show a few cases where an insufficient number of paw-prints or jitters are present and tiles are not fully sampled. By discarding these problematic observations among those that remain only very few need to be re-obtained. Table 7 shows the average seeing, ellipticity, zero-point and limiting magnitude from all VMC images. These parameters have been calculated excluding problematic observations and represent average values regardless of their execution as part of a concatenation, group or monitoring sequence, as well as from the specific requirements of the different VMC fields with respect to crowding.

#### 4. Data archive

The data reduced by the VDFS pipeline at CASU are ingested into the VSA<sup>12</sup> at the Wide Field Astronomy Unit (WFAU) in Edinburgh which is similar to the WFCAM Science Archive (Hambly et al. 2008). At present, these are data reduced with v1.0 of the CASU pipeline and include all VMC data observed until end of May 2010 (Tables 4 and 5). At VSA the data are curated to produce standardised data products. The software that runs at WFAU and populates the VSA is the same that runs at CASU and this guarantees that the data are processed homogeneously throughout the entire processing chain.

The most important processes, available at present, for the VMC survey are: individual passband frame association and source association to provide multi-colour, multi-epoch source lists; cross-association with external catalogues (list-driven matched photometry); deeper stacking in specified fields; quality control procedures.

There are three main types of VSA tables that are important for the VMC survey. These are the *vmcDetection* table, the *vmcSource* table and the *vmcSynoptic* table(s). The *vmcDetection* table contains the catalogues corresponding to individual observations. At the moment there is one catalogue per paw-print, regardless of band and tile of origin. The *vmcSource* table contains the list of sources obtained from deep stack images and each source is matched in the three VMC bands. In practise, each row of the *vmcSource* table will contain *Y*, *J* and *K<sub>s</sub>* magnitudes for a source. At present, because VSA is organised by paw-prints, the same source may appear two or more times in the *vmcSource* table depending on its location with respect to the overlap among the six paw-prints forming a tile. The synoptic tables contain the colour information and the multi-epoch information for individual observations (a single OB). More details about the synoptic tables are given by Cross et al. (2009). The position and magnitude for each source in any given table refers to the astrometrically and photometrically calibrated measurements using the parameters specified in the image headers. These parameters are discussed in Sect. 3. In addition, there are several quality flags that are specifically introduced at the VSA level. These flags identify problems occurring during the ingestion of the data into the archive, incompleteness in the set of data (for example missing exposures in a paw-print sequence), problems related to the pairing of data, etc.

The magnitudes of the brightest stars are corrected for saturation effects (Sect. 3.1). Figure 7 shows the *K<sub>s</sub>* magnitude difference for stars in the 8\_8 field compared to 2MASS before and after saturation correction. Saturation effects are present for *K<sub>s</sub>* < 12 mag, with the magnitudes of brighter stars recovered to at least *K<sub>s</sub>* = 10 mag after correction.

The VSA is queried using Structured Query Language (SQL) and a point-and-click web form for browsing. This is a dual (sophisticated and simple) end-user interface for the data. A key feature to note is the design with multi-waveband catalogue data that allows the user to track back to the individual source images and merged-source tables, and present the user with a generally applicable, science-ready dataset. The VSA has a high-speed query interface, links to analysis tools such as TopCat, and advanced new VO services such as MySpace. The VSA supports a different range of queries and the most common for the VMC survey are: (i) querying the archive to check which data have been ingested; (ii) querying the *vmcSource* table to extract magnitudes from the deep stacks; (iii) querying the synoptic tables

<sup>12</sup> <http://horus.roe.ac.uk/vsa/login.html>

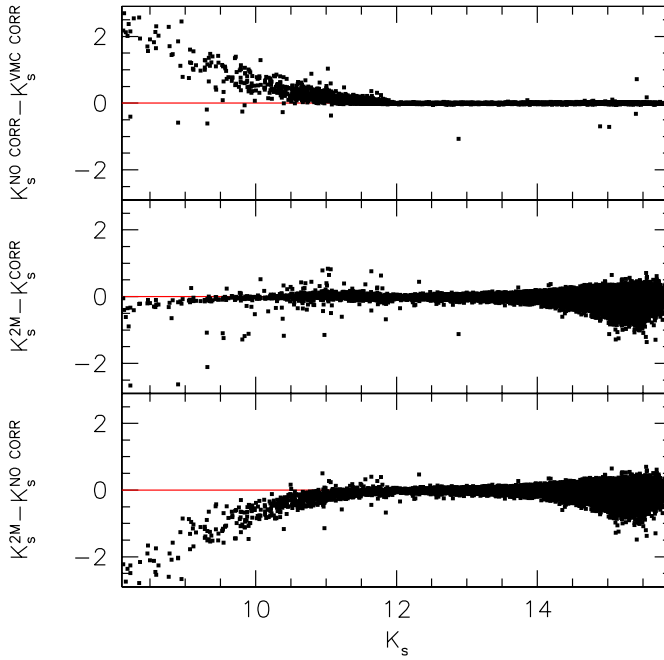


**Fig. 7.** Magnitude difference for stars in the 8\_8 field in common between VMC and 2MASS before (bottom) and after (middle) correcting the magnitude of VMC stars approaching the saturation limit, and (top) the correction itself developed by Irwin (2009).

to extract light-curves and statistics on the levels of variability and (iv) querying the VSA using an input list of sources and searching for their VMC counterpart. For each source in (i) it is possible to inspect postage stamp images in each wave band.

Before creating the deep stack images, the quality control results discussed in Sect. 3.4 need to be taken into account. In particular, all images except those with a large seeing and/or ellipticity listed in Tables 4 and 5 are included in the deep stacks. This means that tile images with a reduced number of jitters or paw-prints are included into the deep stacks if their observing conditions are met. The latter will still be available as individual epochs, and will be linked to the other observations in the synoptic tables, because they may contain useful information for variable stars or for source confirmation.

In the future it may be possible to automatically join the under-exposed areas at the two ends of each tile with those of the adjacent tiles prior to source extraction. The VSA also contains external catalogues, like 2MASS, that can be linked with the VMC data via an SQL query. Catalogues that are specifically important for the Magellanic system, e.g. the MCPS and the SAGE catalogues are also being ingested into the VSA. VMC is intrinsically a multi-wavelength project and a large fraction of its science will come from the linking of VISTA data with those from other surveys; the VSA is designed to enable such links.

## 5. Analysis and results

Figure 8 shows the CMDs of the VMC data in the 6\_6 (30 Dor) and 8\_8 (Gaia) LMC fields. These data were extracted from the VSA. The magnitudes and colours of each source correspond to a single detector, i.e. if the same source was detected in another detector it is not included in the CMDs. This is because at this stage the archiving process is organised by paw-prints. When tiles, resulting from the combination of six paw-prints, become available at VSA then the exposure time per source will be at

least doubled. At present the exposure times per band for the sources (stellar and probably stellar) shown in the CMDs correspond to 1200 s in  $Y$ , 1400 s in  $J$  and to  $\sim 4000$  s in  $K_s$ .

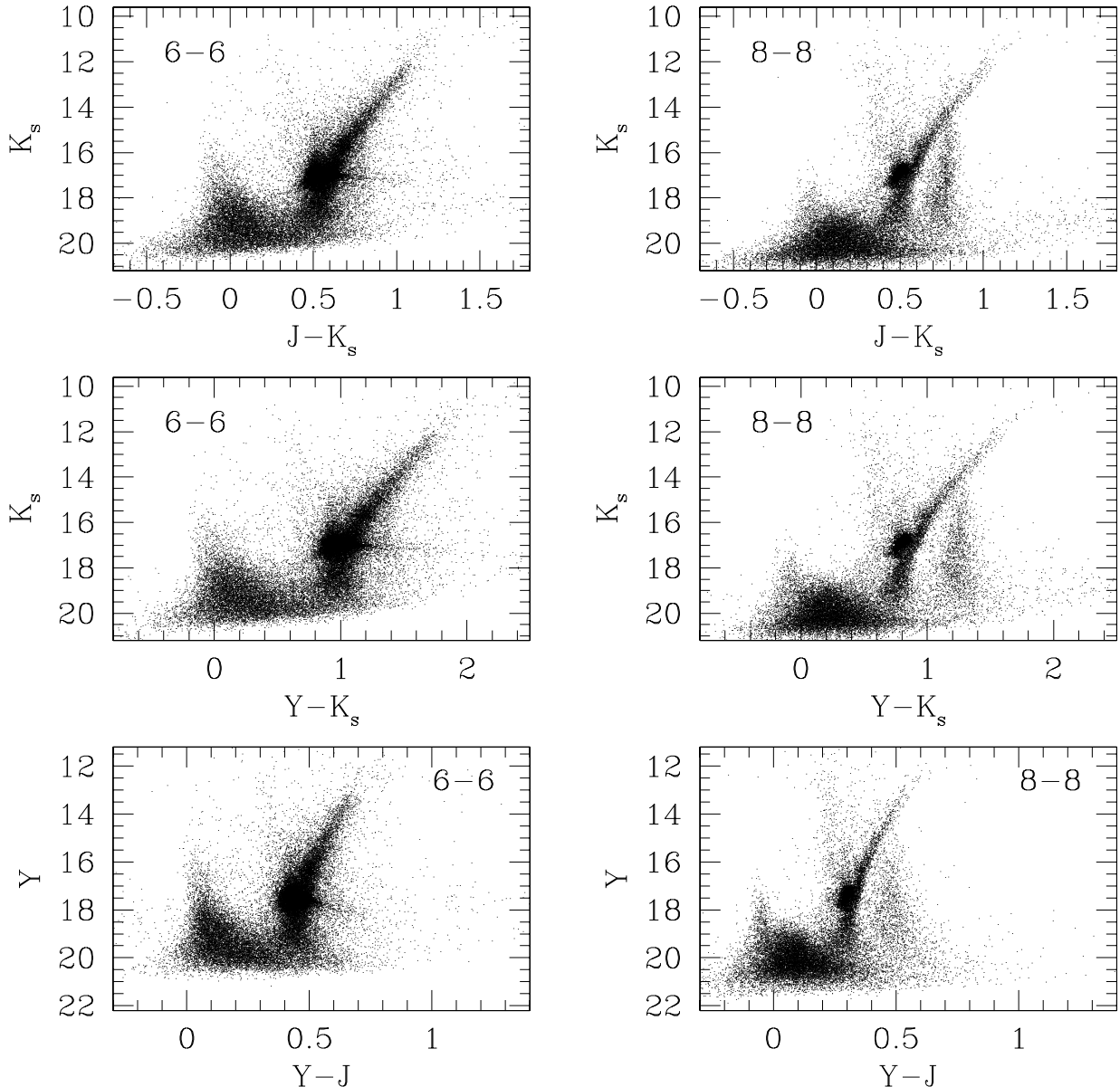
The distribution of stars in the CMDs shows clearly the different stellar populations characterising these LMC fields. The blue-most conic structure bending to red colours at bright magnitudes is formed by main-sequence (MS) stars of increasing mass with increasing brightness. The MS joins, via the sub-giant branch, the RGB beginning at  $\sim 2$  mag below the red clump, the approximately circular region described by the highest concentration of stars. The structure of the red clump depends on stellar parameters (age and metallicity) but also on interstellar extinction. Extinction causes the clump to elongate to red colours, as seen in the CMDs for the 30 Dor field where extinction is higher than in the Gaia field. The RGB continues beyond the red clump at brighter magnitudes describing a narrow structure bending to red colours. The abrupt change in source density at the tip of the RGB marks the transition to brighter AGB stars. The broad vertical distribution of stars below the RGB is populated by MW stars. In the CMDs of the Gaia field these are easily distinguished from LMC stars. Cepheid and supergiant stars occupy the region of the diagram to the bright and blue side of the RGB while RR Lyrae stars are somewhat fainter than the red clump and lie more or less parallel to the sub-giant branch.

Figure 9 shows the colour–colour diagram of the VMC data in the 8\_8 field. The data shown here are the same as in the CMDs (Fig. 8) described above. The distribution of sources in the colour–colour diagram resembles the body of an ant. Following this analogy:

- The lower part of the ant body (*gaster*) at  $-0.1 < (Y - J) < 0.2$ ,  $-0.3 < (J - K_s) < 0.2$ , corresponds to the location of MS stars in the LMC, with the youngest stars being at the bluest extremity. The width of this feature is mainly caused by photometric uncertainties. Its extension to the red is also set by the limited depth of the VMC data, since the faint MS should continue to even redder colours.
- The middle part of the ant body (*mesosoma*) at  $0.2 < (Y - J) < 0.4$ ,  $0.3 < (J - K_s) < 0.65$ , corresponds to the main locus of helium-burning giants in the LMC. The bulk of them are in the red clump (see Fig. 8), but also brighter helium burning giants, and stars in the faint extension of the red clump, fall in this same blob.
- The *petiole* is a small thin extension of the mesosoma at its red side, at  $0.2 < (Y - J) < 0.3$ ,  $0.2 < (J - K_s) < 0.3$ , and is mainly caused by bright stars in the MW foreground – more specifically by the intermediate-age and old turn-offs of MW disk populations (at  $K_s < 15$ ).

In addition to this well-defined petiole, gaster and mesosoma are also connected by the relatively less populated LMC sub-giants, lowest-luminosity RGB stars, and horizontal branch stars in the LMC.

- The upper part of the ant body (*head*) is a more complex feature. Its main blob at  $0.4 < (Y - J) < 0.6$ ,  $0.6 < (J - K_s) < 0.8$  is defined by low-mass stars in the MW foreground, especially those with masses  $< 0.5 M_\odot$  which clump at the same near-IR colours ( $J - K_s \sim 0.7$ ; see Nikolaev & Weinberg 2000; Marigo et al. 2003). The same structure forms a marked vertical feature in the CMDs.
- Two *antennae* depart from this head, the upper one at  $0.5 < (Y - J) < 0.6$ ,  $0.8 < (J - K_s) < 1$  being formed by the more luminous RGB stars in the LMC, close to their tip of the RGB, extending up to  $(J - K_s) = 1$  mag. This upper antenna finishes abruptly because the tip has been reached.



**Fig. 8.** Colour–magnitude diagrams of VMC sources in part of the 6\_6 (30 Dor) and 8\_8 (Gaia SEP) LMC fields.

The lower antenna at  $(J - K_s) \sim 0.8$ ,  $(Y - J) > 0.6$ , is more fuzzy, and corresponds to the  $Y - J$  red-ward extension of low-mass stars in the MW foreground. This red ward extension is partially caused by photometric uncertainties and by the particular colour–colour relation followed by the coolest M dwarfs.

### 5.1. Completeness

Some key science goals of the VMC survey require accurate estimates of the completeness of the stellar photometry as a function of location across the Magellanic system, and position in the CMDs. This is estimated via the usual procedure of adding artificial stars of known magnitudes and positions to the images, then looking for them in the derived photometric catalogues.

For this work, the paw-print images, available for the 8\_8 LMC field, were combined to produce a tile image using the SWARP tool (Bertin et al. 2002). A region of the tile image with a size of  $4000 \times 4000$  pixels was selected. Then, PSF photometry using the DAOPHOT and ADDSTARS packages in IRAF was performed. Figure 10 shows an example of the photometry on the (preliminary) stacked image.

The artificial stars are positioned at the same random position on the  $YJK_s$  images. Their mutual distances are never smaller than 30 pixels, so that the process of adding stars does not increase the typical crowding of the image. Later on, artificial stars spanning small bins of colour and magnitude are grouped together to provide estimates of number ratio between added and recovered stars – i.e. the completeness – as a function of position in the CMDs.

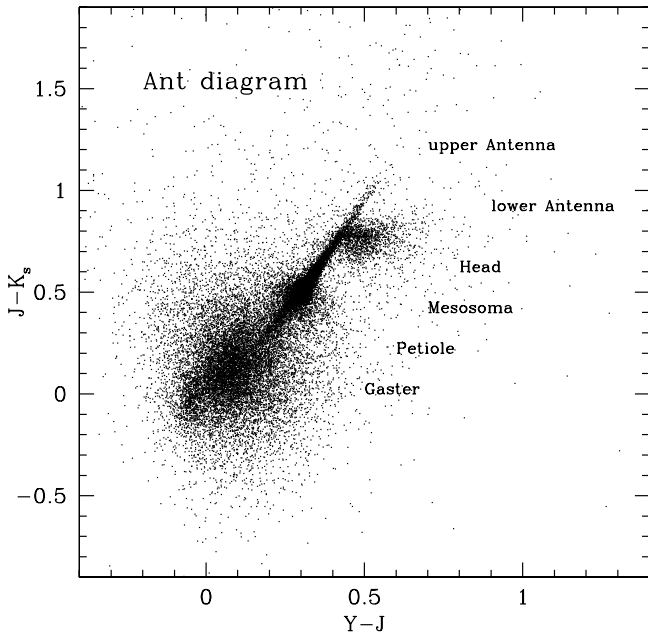


**Fig. 9.** Ant diagram: the colour–colour diagram of VMC sources in part of the 8\_8 LMC field.

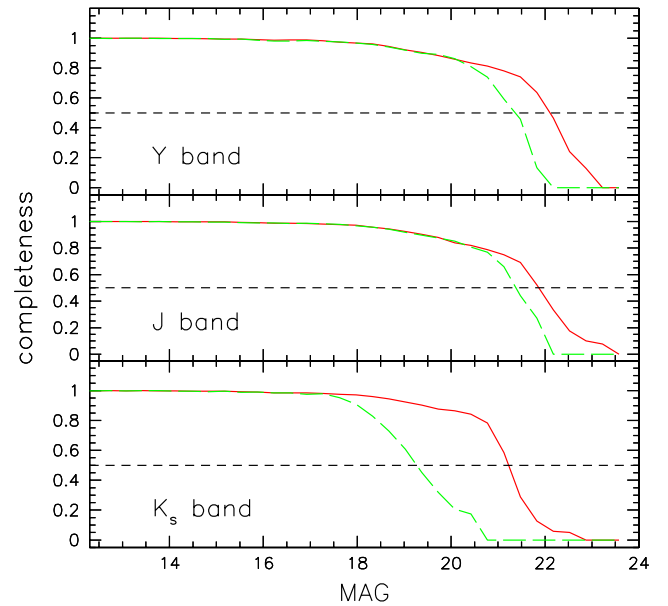


**Fig. 11.** Completeness results for the 8\_8 LMC tile with a single epoch (dashed line) and with deep stacked images (continuous line).

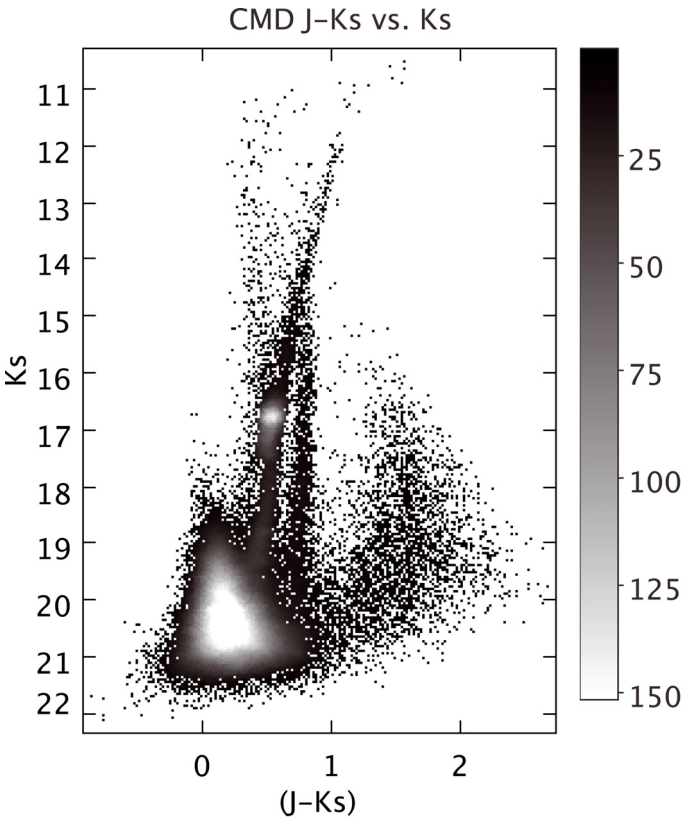


**Fig. 10.** CMD for a region of  $4000 \times 4000$  pixels extracted from the 8\_8 LMC deep tile. Objects with  $J - K_s > 1$  and fainter than  $K_s = 16$  mag are background mostly galaxies.

Typical results of this process are illustrated in Fig. 11, which shows the completeness as a function of magnitude, for both cases of single epoch and deep stacked images. For this relatively low density tile, the figure shows that the  $\sim 50\%$

completeness limit goes as deep as 22.20, 21.90, and 21.40 mag in the  $Y$ ,  $J$  and  $K_s$  bands, respectively. These results are in good agreement with the expectations derived from simulated VMC images (Kerber et al. 2009).

In order to derive the spatially-resolved SFH of the Magellanic Clouds, we are performing a more extensive series of artificial star tests in the available images. The results will be discussed in detail in a forthcoming paper of this series.

### 5.2. RR Lyrae stars and Cepheids

Radially pulsating stars obey a period-mean density relation that forms the basis of their use as standard candles to measure distances to the host systems. RR Lyrae stars in particular, obey a period-luminosity-metallicity (PLZ) relation in the  $K$  band which is weakly affected by evolutionary effects, spread in stellar mass within the instability strip, and uncertainties in reddening corrections (see Longmore et al. 1986, and Sollima et al. 2006 for updates). Similarly, the Cepheid PL relation in the  $K$  band is much narrower than the corresponding optical relations, and less affected by systematic uncertainties in reddening and metal content (Caputo et al. 2000).

The  $K$ -band PLZ relation of RR Lyrae stars has already been used by a number of authors to derive the distance to LMC clusters and field regions (Dall’Ora et al. 2004; Szewczyk et al. 2008; Borissova et al. 2009). However, these studies only cover a few tiny LMC portions mainly located in or close to the LMC bar, and just one LMC cluster, the Reticulum (Dall’Ora et al. 2004). In the context of the VMC project, the  $K_s$  photometry is taken in time series mode in order to obtain mean  $K_s$  magnitudes for RR Lyrae stars and Cepheids over the whole MCs, and use their PL relations to measure distances and construct a 3D map of the entire system.

Over the last decades, large microlensing surveys such as MACHO, EROS and OGLE have been conducted in the optical domain to search for planetary-to-stellar-mass baryonic

dark matter in the MW. As a by-product these surveys have produced tens of millions of light curves of individual background stars. These surveys provide an unprecedented opportunity for systematic studies of whole classes of variable stars and their host galaxies. They cover different fractions of the MC area. Specifically, the MACHO survey (see Alcock et al. 2004, and references therein) cover a region mainly encompassing the LMC and SMC bars. The OGLE surveys (Soszyński et al. 2008, 2009, and references therein) of which stage IV is in progress, cover a progressively larger area extending further outside the bar of each Cloud. EROS-2 (Tisserand et al. 2007) is the most extended of these surveys and, at present, is the one covering the largest fraction of the VMC survey area.

We are using the identification, the period and the epoch of maximum light of RR Lyrae and Cepheids, identified by the microlensing surveys, to fold the  $K_s$ -band light curves produced by VMC and derive average  $K_s$  magnitudes for these variables. In this paper we present results of a preliminary analysis based on the combination of VMC, EROS-2 and OGLE III data for Cepheids and RR Lyrae stars in two LMC fields, namely, the Gaia and 30 Dor fields.

Given its location on the periphery of the LMC, the Gaia field only overlaps with EROS-2. Coordinates, periods and optical<sup>13</sup> light-curve dataset of RR Lyrae and Cepheids in the Gaia field are taken from the EROS-2 catalogue and cross-matched to the VMC data. The 30 Dor field is covered by both EROS-2 and OGLE III, as well as by MACHO, but for the present analysis we only employ periods and optical (Johnson-Cousins  $V, I$  bands) light curves from OGLE III (Soszyński et al. 2008, 2009).

RR Lyrae stars and Cepheids in the Gaia field were extracted from the EROS-2 catalogue and the  $(B - R, R)$  CMD using the following limits:  $18.46 < B < 20.03$  mag,  $0.05 < (B - R) < 0.58$  mag for the RR Lyrae stars, and  $13.39 < B < 17.82$  and  $0.89 < P < 15.85$  days for the Cepheids. This selection returned a list of 16337 RR Lyrae stars and 5800 Cepheids over the whole field of the LMC covered by EROS-2. RR Lyrae candidates and Cepheids within the Gaia field were then extracted according to their coordinates by considering only objects with  $87.8464 < \alpha < 91.8464$  deg and  $-67.3413 < \delta < -65.3413$  deg, giving 235 RR Lyrae and 47 Cepheid candidates. The RR Lyrae candidates were then further selected by considering only objects with “proper” periodicities from EROS-2. This restricted the sample to 218 sources inside the Gaia field. A preliminary cross-match between this catalogue and the VSA<sup>14</sup> was then made using the *CrossID* query (pairing radius 1''), yielding a final catalogue of 117 RR Lyrae candidates and 21 Cepheids in common.

Astrometric differences between the EROS-2 sources and VMC counterparts is  $<1''$  for 98.4% of the sources (with differences for the remainder in excess of 5''). Periods for these stars were checked by analysing their  $B_{\text{EROS}}$  light-curves with Graphical Analyser of Time Series (GRATIS) custom software developed at the Bologna Observatory by Montegriffo (Clementini et al. 2000) confirming the EROS-2 periodicities for the majority. Similar methods were employed to select and cross-match RR Lyrae stars and Cepheids in the 30 Dor field from the OGLE III catalogue, and to extract their  $K_s$  band time series data from the VMC observations.

<sup>13</sup> The EROS *blue* channel (420–720 nm), overlapping the  $V$  and  $R$  standard bands, and *red* channel (620–920 nm), roughly matching the mean wavelength of the Cousins  $I$  band (Tisserand et al. 2007).

<sup>14</sup> Database release VMC20100607.

Figure 12 shows  $B_{\text{EROS}}$  and  $K_s$  VMC light curves of a fundamental mode RR Lyrae star (star #15574, with  $P = 0.601586$  days) and a Cepheid (star #6104, with  $P = 3.87046$  days) in the Gaia field. Also shown are  $V_{\text{OGLE III}}$  and  $K_s$  VMC light-curves of a fundamental mode RR Lyrae star (star #22926, with  $P = 0.5469449$  days) and a Cepheid (star #2871, with  $P = 6.3497921$  days) in the 30 Dor field<sup>15</sup>.

In practise, in the VMC paw-print the same source will (on average) appear in at least one more detector within the same tile sequence; the  $K_s$  magnitudes and uncertainties shown in Fig. 12 for RR Lyrae stars are the weighted averages of all available observations, so for each night we have one point. For the Cepheids all the  $K_s$  data available in the VSA release (VMC20100607) are shown in the figure, i.e., two points for each night, in order to show the excellent raw data for these stars.

Error bars of the individual  $K_s$  measurements are shown in the figures. The uncertainties for the Cepheids in both fields are the same size as the data-points in the figures, while they are larger for the 30 Dor RR Lyrae star due to the crowding in this part of the LMC. Nevertheless, the typical shape of the fundamental mode of the RR Lyrae stars is easily recognised in Fig. 12. The  $K_s$  light-curves are very well sampled for both Cepheids and RR Lyrae stars confirming the soundness of our observing strategy, and allowing us to derive accurate  $\langle K_s \rangle$  magnitudes without using template light curves. The  $\langle K_s \rangle$  magnitudes, computed as the average of the individual  $K_s$  measures correspond to  $18.02 \pm 0.12$  mag,  $17.99 \pm 0.06$  mag for the Gaia and the 30 Dor RR Lyrae stars, respectively, and to  $14.17 \pm 0.06$  mag,  $13.46 \pm 0.08$  mag for the Gaia and the 30 Dor Cepheids, respectively where the quoted uncertainties are the standard deviations of the averages.

The  $\langle K_s \rangle$  magnitudes from the VMC time series will be used along with EROS-2 and OGLE III light-curves to construct  $\text{PL}_{K_s}Z$  relations for the RR Lyrae stars and PL, PL-colour and Wesenheit relations for Cepheids, to then investigate the geometrical distribution of variables in these LMC fields and for the MC system in general.

### 5.3. Planetary nebulae

There are approximately 700 objects catalogued as PNe in the LMC (Leisy et al. 1997; Reid & Parker 2006a,b) and 140 in the SMC (Jacoby, private communication; Sanduleak & MacConnell & Philip 1978; Jacoby 1980; Jacoby & De Marco 2002). Magellanic PNe are best known for their fundamental role in the development of the extragalactic standard candle [O III]  $\lambda 5007$  Planetary Nebula Luminosity Function (PNLF; Henize & Westerlund 1963; Jacoby 1980, 1989). Distances can be measured from the near-universal bright end cut-off across all galaxy types, but it remains difficult to explain how old stellar populations that lack recent star-formation episodes could produce progenitors massive enough to power the high central star luminosities populating the bright end (Jacoby 1997; Marigo et al. 2004; Ciardullo 2010).

Some success in reproducing the observed PNLF has been achieved by incorporating the latest hydrodynamic, time-dependent models (Schönberner et al. 2007; Méndez et al. 2008). In these simulations the emphasis is on modelling the

<sup>15</sup> The variables in the Gaia field have EROS-2 identifications of Im0382m15574 and Im0507l6104 for the RR Lyrae and Cepheid, respectively. Similarly, the variables in the 30 Dor field have OGLE III identifications of OGLE-LMC-RRLYR-22926 and OGLE-LMC-CEP-2871, for the RR Lyrae and Cepheid, respectively.

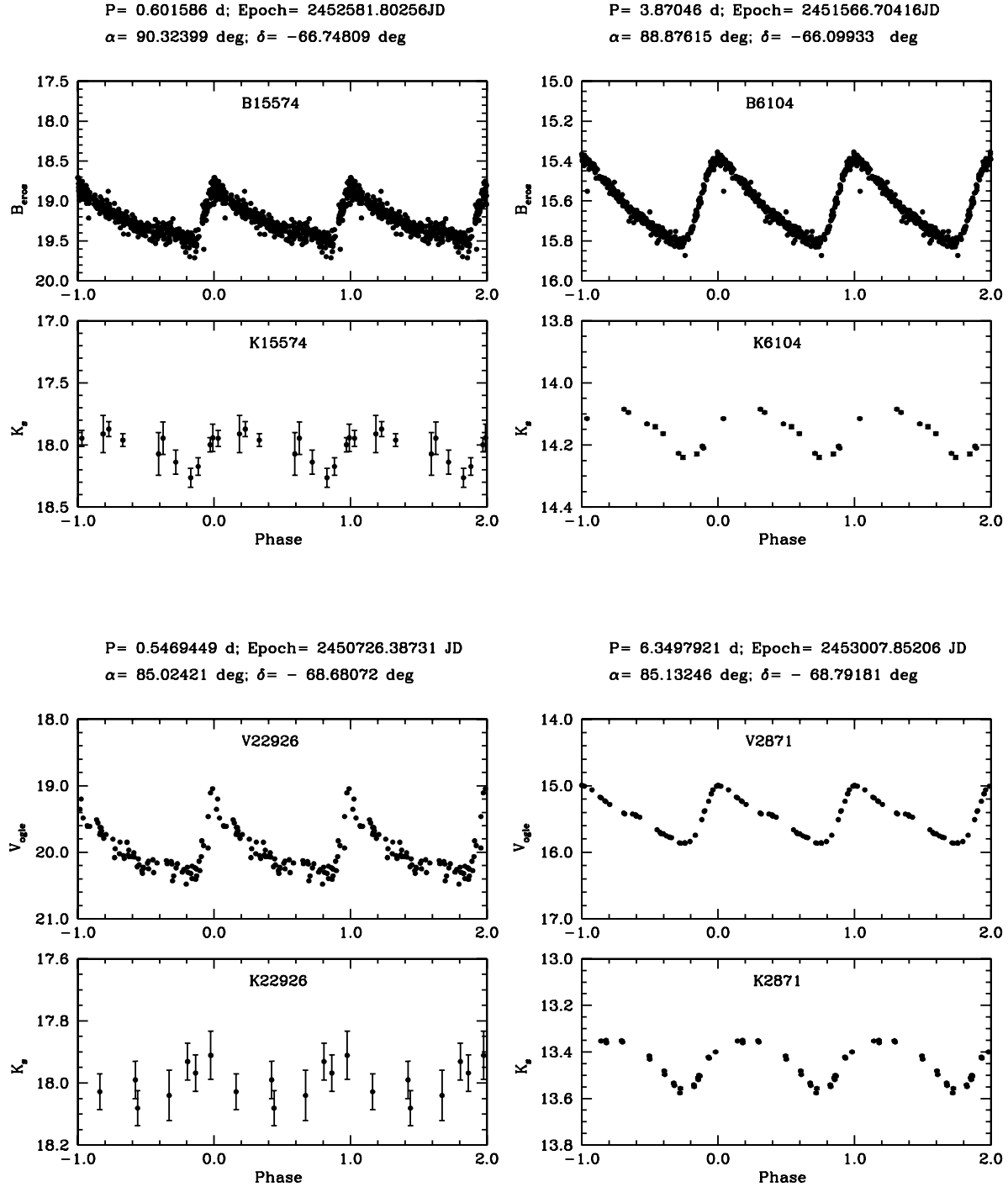


**Fig. 12.**  $B_{\text{EROS}}$  and  $K_s$  VMC light-curves of the fundamental mode RR Lyrae star #15574 and for Cepheid # 6104 in the Gaia SEP field (*top*) as well as  $V_{\text{OGLE III}}$  and  $K_s$  VMC light-curves of the fundamental mode RR Lyrae star #22926 and for Cepheid # 2871 in the 30 Dor field (*bottom*). Data are folded according to the period and epoch of maximum light derived from the EROS-2 data.

PNLF rather than explaining it and an alternative explanation for [O III]-bright PNe is still required. Ciardullo et al. (2005) proposed that blue stragglers could evolve into [O III]-bright PNe provided they are formed via a close binary interaction. Soker (2006) and Frankowski & Soker (2009) suggested symbiotic stars could fulfill the role of [O III]-bright PNe, but this

would controversially require the majority of their nebulae to be ejected by the white dwarf (see Corradi 2003). Both of these scenarios require alternative binary evolution channels for PN formation and as such they are not out of place amongst the growing evidence for binarity in PNe (De Marco 2009). The frequency of PNe with close binary central stars that went

through a common-envelope interaction is fairly high at  $17 \pm 5\%$  (Miszalski et al. 2009) and symbiotic stars could potentially be rebranded as wide interacting binary central stars if we insist upon the nebula origin as already stated. Out of the two scenarios symbiotic stars are more readily accessible despite there being a severe paucity of Magellanic symbiotics (Belczyński et al. 2000).

Magellanic PNe are well positioned to further advance our understanding of the PNLF. Large catalogues of [O III] fluxes are available (Jacoby & De Marco 2002; Reid & Parker 2010) and the MCs are close enough to allow their PNe to be spatially resolved and studied in detail (e.g. Shaw et al. 2006). This is a critical advantage over more distant [O III] selected populations which are frequently assumed to contain only PNe. There are however a large variety of potential mimics that can contaminate the PNLF (see Frew & Parker 2010, for a review) and symbiotic stars have been identified in the Local Group (Gonçalves et al. 2008; Kniazev et al. 2009). Ciardullo (2010) found a large scatter in the emission line ratios of objects in the top magnitude of the M 33 and LMC H $\alpha$  PNLFs which supports the case that more than one type of object can occupy the bright end. The deep near-IR photometry provided by VMC is sensitive to the dust associated with many mimics including compact HII regions and symbiotic stars.

The synoptic nature of the VMC survey will detect variability due to Mira pulsations of the most obscured symbiotic stars that may otherwise be misclassified as PNe. These pulsations may not be visible at optical wavelengths (Mikołajewska et al. 1989) providing a unique opportunity to increase the number of Magellanic symbiotic stars. We might also be sensitive to variability in the brightest central stars that could potentially be evidence for binarity if the variability is later found to be periodic (Miszalski et al. 2009), however only a very small fraction of the population might be expected to fall within our magnitude limits (Villaver et al. 2007).

Within the first six VMC tiles in the LMC, a combination of optical imaging, OGLE light-curves, the VMC near-IR data, and SAGE mid-IR observations, reveals that only  $\sim 50\%$  of the 98 objects catalogued previously as PNe appear to be genuine. These are characterised by the colours  $0.4 \lesssim J - K_s \lesssim 2$  and  $0.0 \lesssim Y - J \lesssim 0.5$ . It is encouraging though that almost all the genuine PNe are detected in all wavebands and they appear especially bright in  $K_s$ . The strongest emission lines in the near-IR for PNe include He I 1.083  $\mu\text{m}$  in  $Y$ , Pa  $\beta$  in  $J$ , while  $K_s$  contains Br  $\gamma$ , multiple He I and molecular H<sub>2</sub> lines (Hora et al. 1999). Figure 13 shows the impact of stacking the individual exposures to detect PNe, many of which are only visible in the stacked frames. The non-PNe identified in the sample are mainly misclassified field stars, compact HII regions or long-period variables. Our small fraction of genuine PNe is real and not just accounted for by non-detections of faint nebulae in the near-IR. It is also preliminary given the statistics are dominated heavily by the 30 Dor 6\_6 tile whose extensive HII emission nebulosity complicates the task of identifying PNe.

As the VMC survey becomes more complete, near-IR luminosity functions will be constructed and compared with their [O III] (Jacoby & De Marco 2002; Reid & Parker 2010) and mid-IR (Hora et al. 2008) counterparts. Improved diagnostic capabilities with the sensitivity of the deep  $K_s$  stacks and SAGE mid-IR photometry will also be applied to discover new PNe inside and especially outside the central  $5 \times 5$  degrees covered by Reid & Parker to create a more complete census of Magellanic PNe with accurate coordinates.

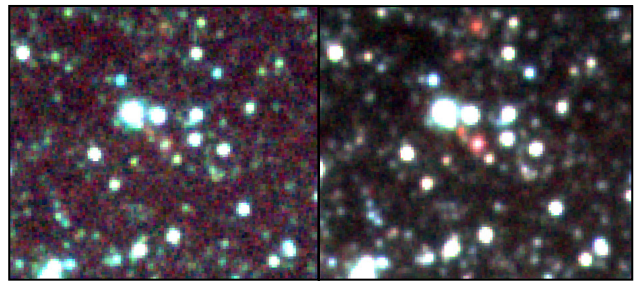


**Fig. 13.** Colour–composite images of the LMC PN MG 60 made from single (left) and stacked (right) exposures of  $Y$  (blue),  $J$  (green) and  $K_s$  (red). The effective exposure times are 200 s for all single exposures, and 2400 s ( $Y$  and  $J$ ) and 6000 s ( $K_s$ ) for the stacked exposures. The images are  $40 \times 35$  arcsec $^2$  with North up and East to the left.

#### 5.4. The stellar cluster KMHK 1577

Stellar clusters are among the primary targets of the VMC survey. The detection of known stellar clusters will be examined, and new clusters will be searched for using a method similar to that already adopted in the study of the MW (Ivanov et al. 2002; Borissova et al. 2003). The analysis of stellar clusters will be centred on the study of CMDs to estimate their ages and metallicities as well as on the comparison with results obtained from optical surveys: MCPS (Zaritsky et al. 2004), OGLE (Pietrzynski et al. 1998, 1999), those by de Grijs & Anders (2006) and other dedicated studies. Ages, masses and metallicities of stellar clusters will allow us to discuss the SFH of the MCs (e.g. synchronised bursts at  $\sim 0.2$  and 2 Gyr between the LMC and the SMC) and radial abundance gradients. The first step of this work has been the compilation of a catalogue of known stellar clusters located in the Gaia SEP and 30 Dor fields from the list of Bica et al. (2008).

In this paper we show preliminary results obtained from the study of one cluster in the 8\_8 field: KMHK 1577. This cluster appears in the literature in different catalogues, including that from Bica et al. (2008), but it is poorly studied and its properties (i.e. age and metallicity) are unknown. It was chosen because of its favourable location at the centre of a VMC paw-print which maximises the availability of data for its stellar members. The VMC observations, available in this field, are listed in Tables 4 and 5. The CMD of the cluster and its immediate surroundings were examined using photometry from deep VSA stacks. The three panels in Fig. 14 show images of the cluster region in the  $Y$ ,  $J$  and  $K_s$  bands where the elliptical region occupied by KMHK 1577 is indicated.

The sources in the cluster region were divided into two concentric groups: an inner group comprising all sources within an ellipse with a major axis of 0.75', a minor axis of 0.70' and a position angle of the major axis of 160° (Bica et al. 2008), and an outer group of sources within a circular area (0.63' in radius) equal in size to twice the area of the inner ellipse. The stars within the elliptical region are likely members of the cluster, although confirmation from radial velocities would be necessary, while stars in the outer region are unlikely associated with the cluster. By extracting the VMC data from the VSA we find 69 sources in the inner group and 98 sources in the outer group. If only sources detected in all three wave bands are considered then there are 41 and 55 sources in the inner and outer group, respectively. The inner group has a higher source density. Using the VSA source classification flag there are 21 stars and 20 galaxies in the inner group and 34 stars and 21 galaxies in

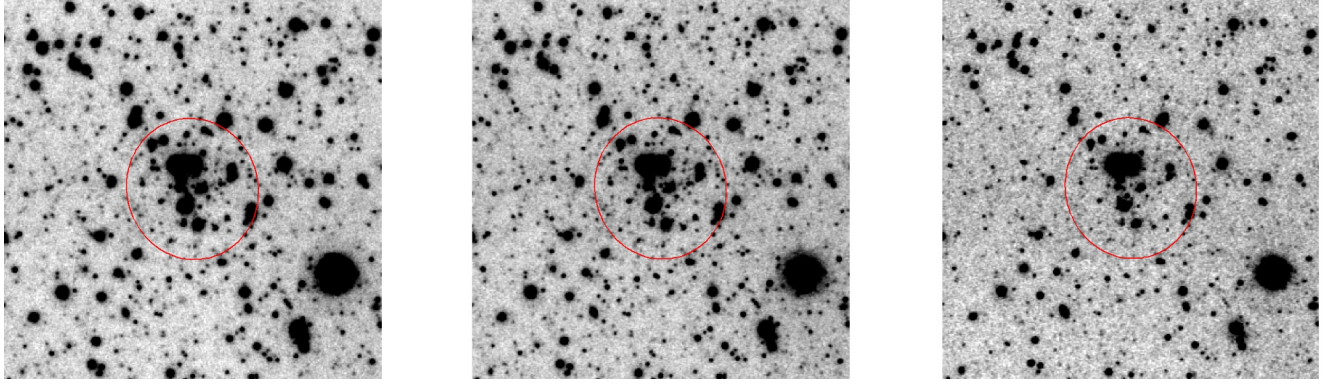


**Fig. 14.** KMHK 1577 observed by VISTA in the  $Y$ ,  $J$  and  $K_s$  bands as part of the VMC survey: these images are about  $2' \times 2'$  in size and refer to 1200, 1400 and  $\sim 4000$  s of integration, respectively. The ellipse shows the size of the cluster as indicated by Bica et al. (2008).

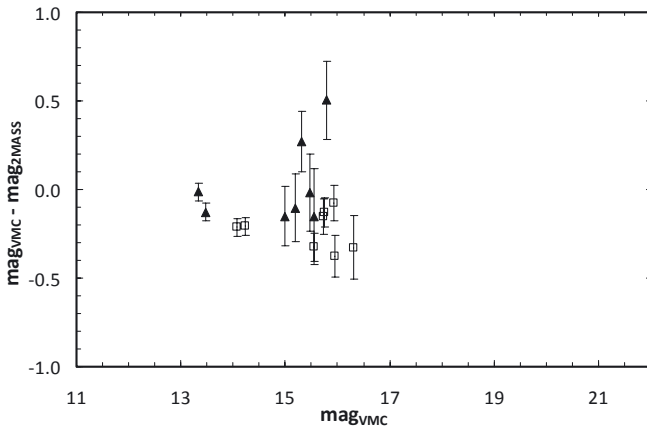


**Fig. 15.** Magnitude differences between 2MASS and VMC detections in the  $J$  (empty squares) and  $K_s$  (filled triangles) bands.

the outer group. Extended objects at faint magnitudes, however, are most probably too faint for the classification criterion into stars and galaxies to work. These objects may be elongated either because of a low signal-to-noise or because they are blends. Their nature will be clearer once all VMC epochs have been obtained and stacked. Only one very bright object is classified as extended and this may be the result of blending in the cluster centre. Objects with red colours and low luminosities are likely extended objects (galaxies, PNe and YSOs), none are present inside the ellipse. Sources in the outer region, that are homogeneously distributed across the area, are either giant stars of the LMC field population or extended objects.

A comparison with 2MASS sources detected within the elliptical region defining the cluster shows that at bright magnitudes ( $K_s \sim 13$ ) there is a very good agreement between the 2MASS and VMC magnitudes, with increasingly discrepant values when approaching the 2MASS sensitivity limit. For the sources in common between VMC and 2MASS (Fig. 15) the magnitude difference in  $J$  and  $K_s$  varies between being practically negligible to values of 0.4–0.5 mag. The difference in the  $J - K_s$  colour is up to 0.8 mag.

The CMD shown in Fig. 16 indicates that the present sensitivity limit of VMC is at  $K_s \sim 21$  mag; this value agrees with expectations. Figure 16 shows that the entire RGB is well detected as well as the sub-giant branch and stars at the MS turn-off point. Photometric uncertainties vary with brightness and in the  $K_s$  band sources with a magnitude of 19–20 have uncertainties of 0.2–0.4 mag, sources with  $16 < K_s < 17$  have uncertainties of

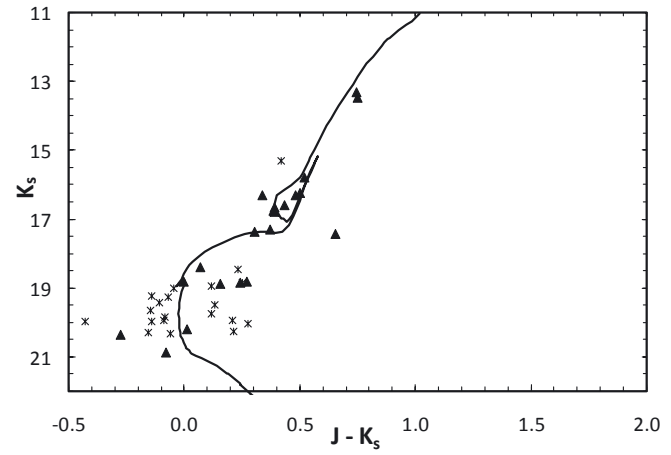


**Fig. 16.** CMD ( $J - K_s$ ,  $K_s$ ) of the inner region around the stellar cluster KMHK 1577. Points represent stellar (filled triangles) and non-stellar (asterisks) objects. The line is the best fit isochrones from Marigo et al. (2008) with an age of 0.63 Gyr and a metallicity of  $Z = 0.003$ .

0.01–0.04 mag and the brightest sources at  $K_s \sim 13$  mag have an uncertainty of  $\sim 0.003$  mag.  $Y$  and  $J$  bands sources have smaller photometric uncertainties than sources in  $K_s$ .

Using theoretical isochrones by Marigo et al. (2008) an age for the cluster of  $0.63 \pm 0.10$  Gyr and a metallicity of  $Z = 0.003 \pm 0.001$  were estimated. These values were derived from the average of the best fit isochrones found in three different CMDs: ( $J - K_s$ ,  $K_s$ ), ( $Y - K_s$ ,  $K_s$ ) and ( $Y - J$ ,  $J$ ). In each of these the best fit age was the same but the metallicity varied within the given dispersion. A similar procedure applied to the outer region gives an older (1.4 Gyr) and more metal poor ( $Z = 0.0004$ ) population. The absorption due to both foreground and interstellar extinction was estimated from  $A_V = 0.55$  mag (Zaritsky et al. 2004) and the  $A_J/A_V$  ratios for an “average” LMC according to Gordon et al. (2003). This results in  $A_Y = 0.22$ ,  $A_J = 0.14$  and  $A_{K_s} = 0.02$  mag where the  $Y$  band value is an extrapolation from the nearest bands. The age of the cluster is typical of young LMC clusters while the low metallicity agrees with the cluster being located in a region quite far from the LMC centre.

Figure 17 shows a CMD ( $B - V$ ,  $B$ ) for the cluster KHM 1577 from the MCPS data (Zaritsky et al. 2004). With reference to the two groups analysed here we find 63 sources in the inner group and 70 sources in the outer group. Although it appears that MCPS has more stars in the central region of the cluster and allows for a better identification of the density enhancement, the VMC data delineate better features in the CMD (compare Fig. 16

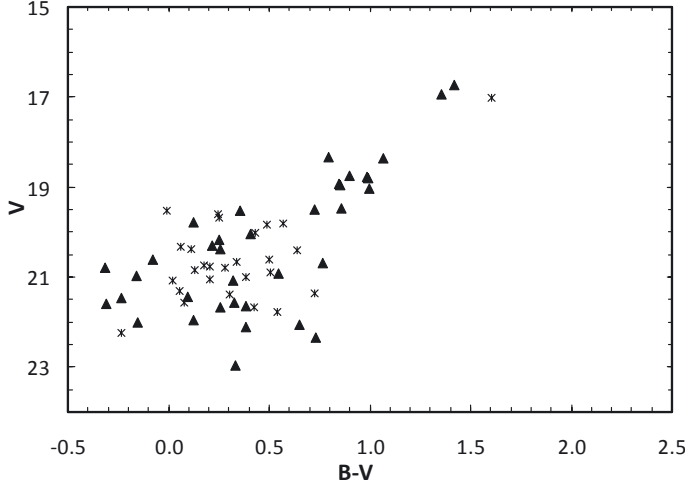


**Fig. 17.** CMD ( $B - V$ ,  $V$ ) obtained from the MCPS data (Zaritsky et al. 2004). Points, for VMC counterparts, are as in Fig. 16.

with Fig. 17). Extinction and crowding effects in the optical data are the most likely explanation for the difference between the two diagrams.

The VMC data harbour a great potential for investigating the evolutionary properties of stellar clusters. The internal spatial distribution of stars for each individual stellar cluster would provide information for dynamical studies.

## 6. Conclusions

The VMC survey is a homogeneous and uniform  $YJK_s$  survey of  $\sim 184$  deg $^2$  across the Magellanic system (Fig. 2). It is an ESO Public Survey that started observations in November 2009 and will run for approximately five years. The VMC survey parameters are described in Table 1. Images and catalogues will be delivered to the astronomical community at regular intervals with the first release expected in 2011. The VMC data will provide, among other things, a detailed history of star formation across the Magellanic system and a measurement of its 3D geometry.

This paper presents the VMC survey strategy and first results aimed at assessing their scientific quality. These show the potential of the survey in addressing its main science goals and validates the expected sensitivity of the VMC data. Colour-magnitude and colour-colour diagrams show a wealth of substructures and a clear separation from Galactic foreground stars. These diagrams will form the core of the SFH analysis. To illustrate some of the scientific applications of the VMC survey, Cepheids and RR Lyrae stars are shown to display clear near-IR light-curves, PNe are detected thanks to the deep  $K_s$  band images dominated by Brγ emission, and stellar cluster parameters are derived from best fit isochrones to the VMC colour-magnitude diagrams.

The VMC survey will be of immense value to the astronomical community because the data will represent the only counterpart for existing optical surveys at a similar sensitivity (e.g. MCPS) and for the large number of unclassified objects observed by the *Spitzer Space Telescope* in the mid-IR (Blum et al. 2006). Note that the near-IR 2MASS survey has observed only about 6% of the stars that the VMC survey is expected to detect. The VMC data cover the bulk of the Magellanic system, as opposed to the tiny regions sampled by the Hubble Space

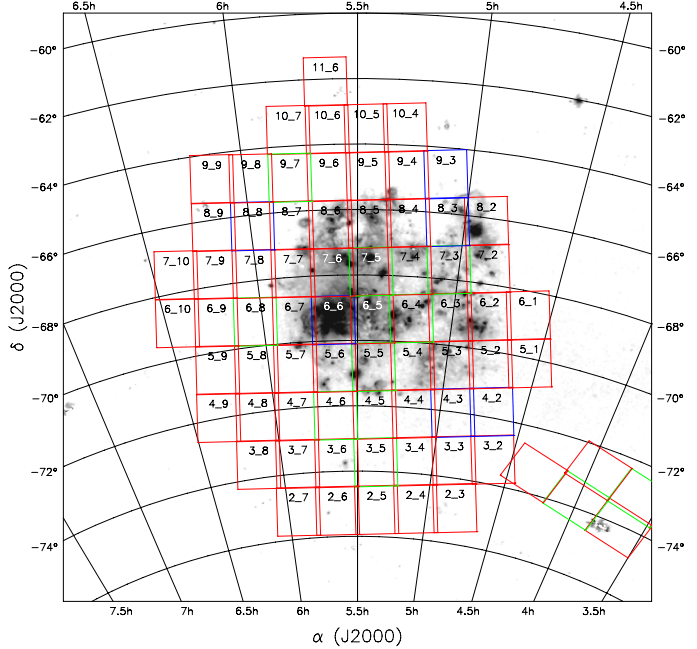


**Fig. A.1.** LMC area tiled for VMC observations. The underlying image shows the H $\alpha$  distribution (Gaustad et al. 2001). VISTA tiles are colour-coded as in Fig. 2.

Telescope, and the limited area covered by most of the other dedicated, ground-based observations at the same sensitivity.

Among the other VISTA Public Surveys, the VISTA Hemisphere Survey (VHS) will also contribute to the investigation of the Magellanic system. The VHS is  $\sim 3$  mag shallower than the VMC survey but it covers an extended area around the Magellanic system to complement the VMC data.

**Acknowledgements.** B.M. thanks George Jacoby for sharing his database of SMC PNe. M.G. and M.A.T.G. acknowledge financial support from the Belgian Federal Science Policy (project MO/33/026). We thank the UK team responsible for the realisation of VISTA, and the ESO team who have been operating and maintaining this new facility. The UK's VISTA Data Flow System comprising the VISTA pipeline at CASU and the VISTA Science Archive at WFAU has been crucial in providing us with calibrated data products for this paper, and is supported by STFC. This research has made use of Aladin, EROS-2 data which were kindly provided by the EROS collaboration and of the Southern H-Alpha Sky Survey Atlas (SHASSA), which is supported by the National Science Foundation. This work was partially supported by PRIN-INAF 2007: “Resolved stellar populations in the near-, mid- and far-infrared (P.I. L. Girardi)” and PRIN-INAF 2008: “The ESO Magellanic Cloud Surveys: tracing the stellar populations and beyond” (P.I. M. Marconi).

## Appendix A: VMC tile centres

Tables A.1 show the centres of VMC tiles covering the LMC, while Table A.2 shows the centres of tiles covering the SMC and Table A.3 shows the centres of tiles covering the Bridge. The tile identification is formed of two numbers. The first number indicates the row and the second number the column that correspond to the location of a given tile. Row numbers increase from bottom to top while column numbers increase from right to left. Refer to Figs. A.1, A.2 and A.3 for the location of tiles across the LMC, SMC and Bridge components of the Magellanic system, respectively. For the Stream the central coordinates of two distinct tiles are indicated in Table A.4. Note that since tiles were generated from almost rectangular grids, some outer tiles were removed leading to the tile numbers shown here.

**Table A.1.** LMC tile centres.

Tile	$\alpha$	$\delta$	Comments
2_3	04:48:04.752	-74:54:11.880	
2_4	05:04:42.696	-75:04:45.120	
2_5	05:21:38.664	-75:10:50.160	
2_6	05:38:43.056	-75:12:21.240	
2_7	05:55:45.720	-75:09:17.280	
3_2	04:37:05.256	-73:14:30.120	
3_3	04:51:59.640	-73:28:09.120	
3_4	05:07:14.472	-73:37:49.800	
3_5	05:22:43.056	-73:43:25.320	started
3_6	05:38:18.096	-73:44:51.000	
3_7	05:53:51.912	-73:42:05.760	
3_8	06:09:16.920	-73:35:12.120	
4_2	04:41:30.768	-71:49:16.320	started
4_3	04:55:19.512	-72:01:53.400	started
4_4	05:09:24.288	-72:10:49.800	
4_5	05:23:39.816	-72:15:59.760	
4_6	05:38:00.408	-72:17:20.040	started
4_7	05:52:20.064	-72:14:49.920	
4_8	06:06:32.952	-72:08:31.200	
4_9	06:20:33.408	-71:58:27.120	
5_1	04:32:43.848	-70:08:40.200	
5_2	04:45:19.440	-70:23:43.800	
5_3	04:58:11.664	-70:35:27.960	
5_4	05:11:16.704	-70:43:46.200	
5_5	05:24:30.336	-70:48:34.200	started
5_6	05:37:47.952	-70:49:49.440	
5_7	05:51:04.872	-70:47:31.200	
5_8	06:04:16.416	-70:41:40.560	
5_9	06:17:18.096	-70:32:20.760	
6_1	04:36:49.488	-68:43:50.880	
6_2	04:48:39.072	-68:57:56.520	
6_3	05:00:42.216	-69:08:54.240	
6_4	05:12:55.800	-69:16:39.360	started
6_5	05:25:16.271	-69:21:08.280	
6_6	05:37:40.008	-69:22:18.120	30 Dor – completed
6_7	05:50:03.168	-69:20:09.240	
6_8	06:02:21.984	-69:14:42.360	started
6_9	06:14:32.832	-69:05:59.640	
6_10	06:26:32.280	-68:54:05.760	
7_2	04:51:34.992	-67:31:57.000	
7_3	05:02:55.200	-67:42:14.760	started
7_4	05:14:23.976	-67:49:30.720	
7_5	05:25:58.440	-67:53:42.000	started
7_6	05:37:35.544	-67:54:47.160	
7_7	05:49:12.192	-67:52:45.480	
7_8	06:00:45.240	-67:47:38.040	
7_9	06:12:11.736	-67:39:26.640	
7_10	06:23:28.800	-67:28:14.880	
8_2	04:54:11.568	-66:05:47.760	
8_3	05:04:53.952	-66:15:29.880	started
8_4	05:15:43.464	-66:22:19.920	
8_5	05:26:37.704	-66:26:15.720	
8_6	05:37:34.104	-66:27:15.840	
8_7	05:48:30.120	-66:25:19.920	
8_8	05:59:23.136	-66:20:28.680	Gaia – completed
8_9	06:10:10.632	-66:12:43.560	
9_3	05:06:40.632	-64:48:40.320	started
9_4	05:16:55.464	-64:55:07.680	
9_5	05:27:14.256	-64:58:49.440	
9_6	05:37:34.872	-64:59:44.520	
9_7	05:47:55.128	-64:57:52.920	in queue

**Table A.1.** continued.

Tile	$\alpha$	$\delta$	Comments
9_8	05:58:12.816	-64:53:15.000	
9_9	06:08:25.848	-64:45:52.560	
10_4	05:18:01.536	-63:27:54.000	
10_5	05:27:48.912	-63:31:22.800	
10_6	05:37:37.800	-63:32:13.200	
10_7	05:47:26.352	-63:30:24.840	
11_6	05:37:42.432	-62:04:41.520	

**Table A.2.** SMC tile centres.

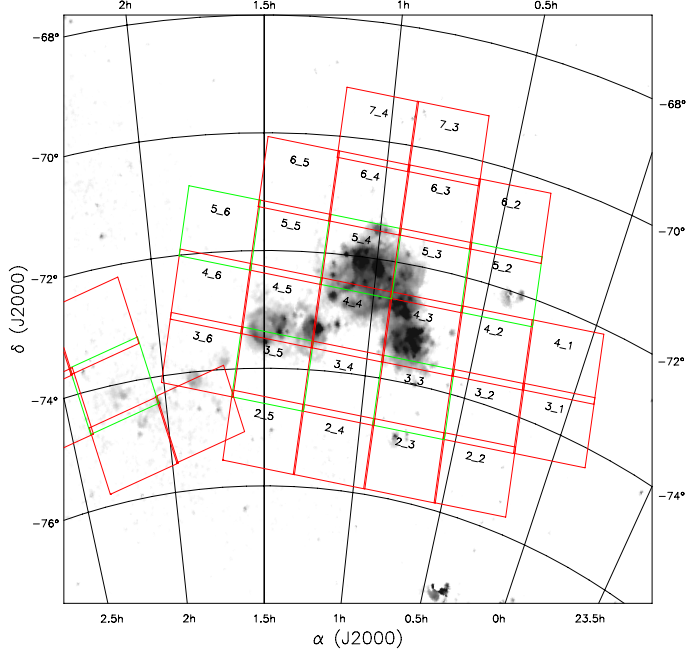
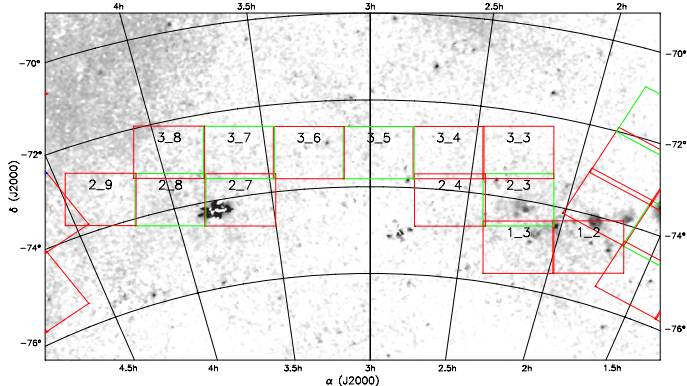
Tile	$\alpha$	$\delta$	Comments
2_2	00:21:43.920	-75:12:04.320	
2_3	00:44:35.904	-75:18:13.320	
2_4	01:07:33.864	-75:15:59.760	
2_5	01:30:12.624	-75:05:27.600	
3_1	00:02:39.912	-73:53:31.920	
3_2	00:23:35.544	-74:06:57.240	
3_3	00:44:55.896	-74:12:42.120	started
3_4	01:06:21.120	-74:10:38.640	
3_5	01:27:30.816	-74:00:49.320	started
3_6	01:48:06.120	-73:43:28.200	
4_1	00:05:33.864	-72:49:12.000	
4_2	00:25:14.088	-73:01:47.640	
4_3	00:45:14.688	-73:07:11.280	in queue
4_4	01:05:19.272	-73:05:15.360	NGC 419
4_5	01:25:11.088	-72:56:02.760	in queue
4_6	01:44:34.512	-72:39:44.640	
5_2	00:26:41.688	-71:56:35.880	started
5_3	00:45:32.232	-72:01:40.080	
5_4	01:04:26.112	-71:59:51.000	NGC 411 – started
5_5	01:23:09.336	-71:51:09.720	
5_6	01:41:28.800	-71:35:47.040	started
6_2	00:28:00.192	-70:51:21.960	
6_3	00:45:48.792	-70:56:09.240	in queue
6_4	01:03:40.152	-70:54:25.200	
6_5	01:21:22.560	-70:46:11.640	in queue
7_3	00:46:04.728	-69:50:38.040	
7_4	01:03:00.480	-69:48:58.320	

**Table A.3.** Bridge tile centres.

Tile	$\alpha$	$\delta$	Comments
1_2	01:49:51.960	-74:43:31.800	
1_3	02:11:35.232	-75:05:04.560	
2_3	02:14:46.584	-74:00:47.520	started
2_4	02:35:28.440	-74:13:18.840	in queue
2_7	03:39:43.800	-74:04:51.960	in queue
2_8	04:00:21.072	-73:46:37.560	started
2_9	04:20:05.640	-73:21:14.040	
3_3	02:17:35.496	-72:56:22.200	
3_4	02:37:24.888	-73:08:16.440	
3_5	02:57:33.288	-73:12:52.200	started
3_6	03:17:43.776	-73:10:03.720	
3_7	03:37:39.240	-72:59:54.600	started
3_8	03:57:03.888	-72:42:37.800	

**Table A.4.** Stream tile centres.

Tile	$\alpha$	$\delta$	Comments
1_1	03:30:03.87	-64:25:24.8	started
2_1	00:11:59.30	-64:39:31.8	started

**Fig. A.2.** SMC area tiled for VMC observations. The underlying image shows the H $\alpha$  distribution (Gaustad et al. 2001). VISTA tiles are colour-coded as in Fig. 2.**Fig. A.3.** Bridge area tiled for VMC observations. The underlying image shows the H $\alpha$  distribution (Gaustad et al. 2001). VISTA tiles are colour-coded as in Fig. 2.

## References

- Alcock, C., Allsman, R. A., Alves, D. R., et al. 2000, ApJ, 542, 281  
 Alcock, C., Alves, D. R., Axelrod, T. S., et al. 2004, AJ, 127, 334  
 Arnaboldi, M., Dietrich, J., Hatziminaoglou, E., et al., 2008, The Messenger, 134, 42  
 Arnaboldi, M., Petr-Gotzens, M., & Rejkuba, M. 2010, The Messenger, 139, 6  
 Barnes, J. E., & Hernquist, L. 1992, Nature, 360, 715  
 Battinelli, P., & Demers, S. 1992, AJ, 104, 1458  
 Battinelli, P., & Demers, S. 1998, AJ, 115, 1472  
 Belczyński, K., Mikołajewska, J., Munari, U., et al. 2000, A&AS, 146, 407  
 Bertin, E., Mellier, Y., Radovich, M., & Missonnier, G. 2002, in Astronomical Data Analysis Software and Systems XI, ASPCS, 281, 228  
 Besla, G., Kallivayalil, N., Hernquist, L., et al. 2007, ApJ, 668, 949  
 Besla, G., Kallivayalil, N., Hernquist, L., et al. 2010, ApJ, 721, L97  
 Bica, E., Bonatto, C., Dutra, C. M., & Santos, J. F. C. 2008, MNRAS, 389, 678  
 Blum, R. D., Mould, J. R., Olsen, K. A., et al. 2006, AJ, 132, 2034  
 Bolatto, A. D., Simon, J. D., Stanimirović, S., et al. 2007, ApJ, 655, 212  
 Bonanos, A. Z., Lennon, D. J., Köhlinger, F., et al. 2010, AJ, 140, 416  
 Bonnarel, F., Fernique, P., Bienaymé, O., et al. 2000, A&ASS, 143, 33  
 Borissova, J., Peshev, P., Ivanov, V. D., et al. 2003, A&A, 411, 83  
 Borissova, J., Rejkuba, M., & Minniti, D. 2009, A&A, 502, 505  
 Bothun, G. D., & Thompson, I. B. 1988, AJ, 96, 877  
 Calabretta, M. R., & Greisen, E. W. 2002, A&A, 395, 1077  
 Capaccioli, M., Mancini, D., & Sedmak, G. 2005, The Messenger, 120, 10  
 Caputo, F., Marconi, M., & Musella, I. 2000, A&A, 354, 610  
 Carrera, R., Gallart, C., Aparicio, A., et al. 2008, AJ, 136, 1039  
 Ciardullo, R. 2010, PASA, 27, 149  
 Ciardullo, R., Sigurdsson, S., Feldmeier, J. J., & Jacoby, G. H. 2005, ApJ, 629, 499  
 Cioni, M.-R. L., Loup, C., & Habing, H. J. 2000a, A&AS, 144, 235  
 Cioni, M.-R. L., van der Marel, R. P., Loup, C., & Habing, H. J. 2000b, A&A, 359, 601  
 Cioni, M.-R. L., Bekki, K., Clementini, G., et al. 2008, PASA, 25, 121  
 Clementini, G., Di Tomaso, S., Di Fabrizio, L., et al. 2000, AJ, 120, 2054  
 Cole, A. A., Tolstoy, E., Gallagher, J. S., & Smecker-Hane, T. A. 2005, AJ, 129, 1465  
 Corradi, R. L. M. 2003, ASPC Series, 303, 393  
 Cross, N. J. G., Collins, R. S., Hambly, N. C., et al. 2009, MNRAS, 399, 1730  
 Dall'Ora, M., Storm, J., Bono, G., et al. 2004, ApJ, 610, 269  
 Dalton, G. B., Caldwell, M., Ward, A. K., et al. 2006, SPIE, 6269, 62690X  
 de Grijts, R., & Anders, P. 2006, MNRAS, 366, 295  
 De Marco, O. 2009, PASP, 121, 316  
 D'Onghia, E., & Lake, G. 2008, AJ, 686, L61  
 Emerson, J., & Sutherland, W. 2010, The Messenger, 139, 2  
 Emerson, J., McPherson, A., & Sutherland, W. 2006, The Messenger, 126, 41  
 Frankowski, A., & Soker, N. 2009, ApJL, 703, L95  
 Frew, D. J., & Parker, Q. A. 2010, PASA, 27, 129  
 Gallart, C., Stetson, P. B., Meschin, I., et al. 2008, ApJ, 682, L89  
 Gaustad, J. E., McCullough, P. R., Rosing, W., & Van Buren, D. 2001, PASP, 113, 1326  
 Gonçalves, D. R., Magrini, L., Munari, U., et al. 2008, MNRAS, 391, L84  
 Gonidakis, I., Livanou, E., Kontizas, E., et al. 2009, A&A, 496, 375  
 Gordon, K. D., Clayton, G. C., Misselt, K. A., et al. 2003, ApJ, 594, 279  
 Gordon, K. D., Bot, C., Muller, E., et al. 2009, ApJ, 690, L76  
 Groenewegen, M. A. T. 2000, A&A, 363, 901  
 Guhathakurta, P., & Reitzel, D. B. 1998, ASP Conf. Ser., 136, 22  
 Hambly, N. C., Collins, R. S., Cross, N. J. G., et al. 2008, MNRAS, 384, 637  
 Harris, J. 2007, ApJ, 658, 345  
 Hatzidimitriou, D., Stanimirović, S., Maragoudaki, F., et al. 2005, MNRAS, 360, 117  
 Henize, K. G., & Westerlund, B. E. 1963, ApJ, 137, 747  
 Hill, V., François, P., Spite, M., et al. 2000, A&A, 364, L19  
 Hodgkin, S. T., Irwin, M. J., Hewett, P. C., & Warren, S. J. 2009, MNRAS, 394, 675  
 Hora, J. L., Latter, W. B., & Deutsch, L. K., 1999, ApJS, 124, 195  
 Hora, J. L., Cohen, M., Ellis, R. G., et al. 2008, AJ, 135, 726  
 Ibata, R. A., Gilmore, G., & Irwin, M. J. 1994, Nature, 370, 194  
 Ibata, R. A., Irwin, M. J., Lewis, G. F., et al. 2003, MNRAS, 340, L21  
 Irwin, M. 1991, IAU, 148, 453  
 Irwin, M. J. 2009, UKIRT Newsletter, 25, 15  
 Irwin, M. J. 2010, UKIRT Newsletter, 26, 14  
 Irwin, M. J., Kunkel, W. E., Demers, A., 1985, Nature, 318, 160  
 Irwin, M. J., Lewis, J., Hodgkin, S., et al. 2004, SPIE, 5493, 411  
 Ivanov, V. D., Borissova, J., Peshev, P., et al. 2002, A&A, 394, L1  
 Jacoby, G. H. 1980, ApJS, 42, 1  
 Jacoby, G. H. 1989, ApJ, 339, 39  
 Jacoby, G. H. 1997, Planetary Nebulae, 180, 448  
 Jacoby, G. H., & De Marco, O. 2002, AJ, 123, 269  
 Kallivayalil, N., van der Marel, R. P., Alcock, C., et al. 2006a, ApJ, 638, 772  
 Kallivayalil, N., van der Marel, R. P., & Alcock, C. 2006b, ApJ, 652, 1213  
 Kato, D., Nagashima, C., Nagayama, T., et al. 2007, PASJ, 59, 615  
 Kerber, L. O., Girardi, L., Ruble, S., & Cioni, M.-R. L. 2009, A&A, 499, 697  
 Knabe, A., Power, C., Gill, S. P. D., & Gibson, B. K. 2006, MNRAS, 368, 741  
 Kniazev, A. Y., et al. 2009, MNRAS, 395, 1121  
 Lasker, B. M., Lattanzi, M. G., McLean, B. J., et al. 2008, AJ, 136, 735  
 Leisy, P., Dennefeld, M., Alard, C., & Guibert, J. 1997, A&AS, 121, 407  
 Longmore, A. J., Fernley, J. A., & Jameson, R. F. 1986, MNRAS, 220, 279  
 Marigo, P., Girardi, L., & Chiosi, C. 2003, A&A, 403, 225  
 Marigo, P., Girardi, L., Weiss, A., et al. 2004, A&A, 423, 995  
 Marigo, P., Girardi, L., Bressan, A., et al. 2008, A&A, 482, 883  
 Mastropietro, C. 2009, IAU, 257, 117  
 Mastropietro, C., Moore, B., Mayer, L., et al. 2005, MNRAS, 363, 509

- McClure-Griffiths, N. M., Pisano, D. J., Calabretta, M. R., et al. 2009, ApJS, 181, 398
- Meixner, M., Gordon, K. D., Indebetouw, R., et al. 2006, AJ, 132, 2268
- Méndez, R. H., Teodorescu, A. M., Schönberner, D., et al. 2008, ApJ, 681, 325
- Mikołajewska, J., Brandt, E., Hack, W., Väistönen, P., & Whitelock, P. A. 1999, MNRAS, 305, 190
- Miszalski, B., Acker, A., Moffat, A. F. J., et al. 2009, A&A, 496, 813
- Moss, C. 2006, MNRAS, 373, 167
- Muller, E., Staveley-Smith, L., Zealey, W., & Stanimirović, S. 2003, MNRAS, 339, 105
- Nikolaev, S., & Weinberg, M. D. 2000, ApJ, 542, 804
- Niedever, D. L., Majewski, S. R., & Burton, W. B. 2008, AJ, 679, 432
- Nishiyama, S., Haba, Y., Kato, D., et al. 2007, ApJ, 658, 358
- Pietrzynski, G., Udalski, A., Kubiak, M., et al. 1998, AcA, 48, 175
- Pietrzynski, G., Udalski, A., Kubiak, M., et al. 1999, AcA, 49, 521
- Pompéia, L., Hill, V., Spite, M., et al. 2008, A&A, 480, 379
- Reid, W. A., & Parker, Q. A. 2006a, MNRAS, 365, 401
- Reid, W. A., & Parker, Q. A. 2006b, MNRAS, 373, 521
- Reid, W. A., & Parker, Q. A. 2010, MNRAS, 405, 1349
- Saha, A., & the OLS Team 2010, NOAO/NSO Newsletter, 101, 4
- Sanduleak, N., MacConnell, D. J., & Philip, A. G. D. 1978, PASP, 90, 621
- Schönberner, D., Jacob, R., Steffen, M., & Sandin, C., 2007, A&A, 473, 467
- Shaw, R. A., Stanghellini, L., Villaver, E., & Mutchler, M. 2006, ApJS, 167, 201
- Schwering, P. B. W. 1989, A&AS, 79, 105
- Soker, N. 2006, ApJ, 640, 966
- Skrutskie, M. F., Cutri, R. M., Stiening, R., et al. 2006, AJ, 131, 1163
- Sollima, A., Cacciari, C., & Valenti, E. 2006, MNRAS, 372, 1675
- Soszyński, I., Poleski, R., Udalski, A., et al. 2008, Acta Astron., 58, 163
- Soszyński, I., Udalski, A., Szymański, M. K., et al. 2009, Acta Astron., 59, 1
- Spergel, D. N., Verde, L., Peiris, H. V., et al. 2003, ApJS, 148, 175
- Staveley-Smith, L., Kim, S., Calabretta, M. R., et al. 2003, MNRAS, 339, 87
- Subramanian, A., & Subramanian, S. 2009b, ApJ, 703, L37
- Subramanian, S., & Subramanian, A., 2009a, A&A, 496, 399
- Subramanian, S., & Subramanian, A. 2010, A&A, 520, 24
- Szewczyk, O., Pietrzynski, G., Gieren, W., et al. 2008, AJ, 136, 272
- Tisserand, P., Le Guillou, L., Afonso, C., et al. 2007, A&A, 469, 387
- Tolstoy, E., Hill, V., & Tosi, M. 2009, ARA&A, 47, 371
- Tully, R., Brent, R., & Dolphin, A. E., et al. 2006, AJ, 132, 729
- Udalski, A., Szymański, M., Kahuńy, J., et al. 1992, Acta Astron., 49, 201
- van der Marel, R. P. 2001, AJ, 122, 1827
- van der Marel, R. P., & Cioni, M.-R. L. 2001, AJ, 122, 1807
- Villaver, E., Stanghellini, L., & Shaw, R. A. 2007, ApJ, 656, 831
- Westerlund, B. E. 1997, in The Magellanic Clouds (Cambridge University Press)
- White, S. D. M., & Frenk, C. S. 1991, ApJ, 379, 52
- Yang, Y., & Hammer, F. 2010, ApJ, 725, L24
- York, D. G., Adelman, J., Anderson, J. E. Jr., et al. 2000, AJ, 120, 1579
- Zaritsky, D., Harris, J., Grebel, E. K., & Thompson, I. B. 2000, AJ, 534, L53
- Zaritsky, D., Harris, J., Thompson, I. B., et al. 2002, AJ, 123, 855
- Zaritsky, D., Harris, J., Thompson, I. B., & Grebel, E. K. 2004, AJ, 128, 1606
- <sup>2</sup> University Observatory Munich, Scheinerstrasse 1, 81679 München, Germany
- <sup>3</sup> INAF, Osservatorio Astronomico di Bologna, via Ranzani 1, 40127 Bologna, Italy
- <sup>4</sup> INAF, Osservatorio Astronomico di Padova, Vicolo dell’Osservatorio 5, 35122 Padova, Italy
- <sup>5</sup> Royal Observatory of Belgium, Ringlaan 3, 1180 Uccle, Belgium
- <sup>6</sup> University of Bologna, Department of Astronomy, via Ranzani 1, 40127 Bologna, Italy
- <sup>7</sup> INAF, Osservatorio Astronomico di Capodimonte, via Moiariello 16, 80131 Napoli, Italy
- <sup>8</sup> ICRAR, M468, University of Western Australia, 35 Stirling Hwy, Crawley 6009, Western Australia
- <sup>9</sup> University of Edinburgh, Institute for Astronomy, Blackford Hill, Edinburgh EH9 3HJ, UK
- <sup>10</sup> University of Cape Town, Private Bag X3, Rondebosch 7701, South Africa
- <sup>11</sup> Peking University, Kavli Institute for Astronomy and Astrophysics, Yi He Yuan Lu 5, Hai Dian District, Beijing 100871, PR China
- <sup>12</sup> Queen Mary University of London, Mile End Road, London E1 4NS, UK
- <sup>13</sup> UK Astronomy Technology Centre, Blackford Hill, Edinburgh EH9 3HJ, UK
- <sup>14</sup> Centre for Astrophysics, University of Central Lancashire, Preston PR1 2HE, UK
- <sup>15</sup> University of Cambridge, Institute of Astronomy, Madingley Rd, Cambridge CB3 0HA, UK
- <sup>16</sup> European Southern Observatory, Av. Alonso de Córdoba 3107, Casilla 19, Santiago, Chile
- <sup>17</sup> UPMC Univ. Paris 06, UMR7095, Institut d’Astrophysique de Paris, 75014 Paris, France
- <sup>18</sup> CNRS, UMR7095, Institut d’Astrophysique de Paris, 75014 Paris, France
- <sup>19</sup> LERMA, Observatoire de Paris, UPMC, CNRS, 61 Av. de l’Observatoire, 75014 Paris, France
- <sup>20</sup> University of Zurich, Institute for Theoretical Physics, 8057 Zurich, Switzerland
- <sup>21</sup> University of Exeter, School of Physics, Stocker Road, Exeter EX4 4QL, UK
- <sup>22</sup> University of Keele, School of Physical and Geographical Sciences, Staffordshire ST5 5BG, UK
- <sup>23</sup> University of Leicester, University Road, Leicester LE1 7RH, UK
- <sup>24</sup> Mount Stromlo Observatory, RSAA, Cotter Road, Weston Creek, ACT 2611, Australia

<sup>1</sup> University of Hertfordshire, Physics Astronomy and Mathematics, Hatfield AL10 9AB, UK  
e-mail: m.cioni@herts.ac.uk